ARTICLE

Variants in the Oxidoreductase PYROXD1 Cause Early-Onset Myopathy with Internalized Nuclei and Myofibrillar Disorganization

Gina L. O'Grady,[1,2,3,25] Heather A. Best,[1,2,25] Tamar E. Sztal,[4,25] Vanessa Schartner,[5,26] Myriam Sanjuan-Vazquez,[6,26] Sandra Donkervoort,[7,26] Osorio Abath Neto,[5] Roger Bryan Sutton,[8] Biljana Ilkovski,[1] Norma Beatriz Romero,[9,10] Tanya Stojkovic,[10] Jahannaz Dastgir,[7] Leigh B. Waddell,[1] Anne Boland,[11] Ying Hu,[7] Caitlin Williams,[4] Avnika A. Ruparelia,[4] Thierry Maisonobe,[10] Anthony J. Peduto,[12] Stephen W. Reddel,[13] Monkol Lek,[14,15] Taru Tukiainen,[14,15] Beryl B. Cummings,[14,15] Himanshu Joshi,[1] Juliette Nectoux,[16,17] Susan Brammah,[18] Jean-François Deleuze,[11] Viola Oorschot Ing,[19] Georg Ramm,[19,20] Didem Ardicli,[21] Kristen J. Nowak,[22] Beril Talim,[21] Haluk Topaloglu,[21] Nigel G. Laing,[22] Kathryn N. North,[1,23] Daniel G. MacArthur,[14,15] Sylvie Friant,[6] Nigel F. Clarke,[1,2] Robert J. Bryson-Richardson,[4] Carsten G. Bönnemann,[7] Jocelyn Laporte,[5,24,27] and Sandra T. Cooper[1,2,27,*]

This study establishes *PYROXD1* variants as a cause of early-onset myopathy and uses biospecimens and cell lines, yeast, and zebrafish models to elucidate the fundamental role of *PYROXD1* in skeletal muscle. Exome sequencing identified recessive variants in *PYROXD1* in nine probands from five families. Affected individuals presented in infancy or childhood with slowly progressive proximal and distal weakness, facial weakness, nasal speech, swallowing difficulties, and normal to moderately elevated creatine kinase. Distinctive histopathology showed abundant internalized nuclei, myofibrillar disorganization, desmin-positive inclusions, and thickened Z-bands. PYROXD1 is a nuclear-cytoplasmic pyridine nucleotide-disulphide reductase (PNDR). PNDRs are flavoproteins (FAD-binding) and catalyze pyridine-nucleotide-dependent (NAD/NADH) reduction of thiol residues in other proteins. Complementation experiments in yeast lacking glutathione reductase *glr1* show that human PYROXD1 has reductase activity that is strongly impaired by the disease-associated missense mutations. Immunolocalization studies in human muscle and zebrafish myofibers demonstrate that PYROXD1 localizes to the nucleus and to striated sarcomeric compartments. Zebrafish with *ryroxD1* knock-down recapitulate features of PYROXD1 myopathy with sarcomeric disorganization, myofibrillar aggregates, and marked swimming defect. We characterize variants in the oxidoreductase *PYROXD1* as a cause of early-onset myopathy with distinctive histopathology and introduce altered redox regulation as a primary cause of congenital muscle disease.

Introduction

Myopathies are a group of genetically heterogeneous conditions characterized by muscle weakness, with overlap in the clinical presentation and histopathological features of different genetic subtypes.[1] Within this group, congenital myopathies are most commonly characterized by hypotonia and weakness, often from birth, commonly with the presence of facial weakness, with or without ptosis and ophthalmoplegia. There are 25 recognized genetic causes of congenital myopathy (see GeneTable in Web Resources); currently a genetic diagnosis is achieved in only ~50% of

[1]Institute for Neuroscience and Muscle Research, Kid's Research Institute, Children's Hospital at Westmead, Sydney, NSW 2145, Australia; [2]Discipline of Paediatrics and Child Health, Faculty of Medicine, University of Sydney, Sydney, NSW 2006, Australia; [3]Paediatric Neurology Service, Starship Children's Health, Auckland 1023, New Zealand; [4]School of Biological Sciences, Monash University, Melbourne, VIC 3800, Australia; [5]Institut de Génétique et de Biologie Moléculaire et Cellulaire (IGBMC), 67400 Illkirch, France; [6]Department of Molecular and Cellular Genetics, UMR7156, Université de Strasbourg, CNRS, Strasbourg 67081, France; [7]National Institute of Neurological Disorders and Stroke Neurogenetics Branch, Neuromuscular and Neurogenetic Disorders of Childhood Section, NIH, Bethesda, MD 20892-1477, USA; [8]Department of Cell Physiology and Molecular Biophysics, and Center for Membrane Protein Research, Texas Tech University Health Sciences Center, Lubbock, TX 79430, USA; [9]Sorbonne Universités, UPMC Univ Paris 06, INSERM UMRS974, CNRS FRE3617, Center for Research in Myology, GH Pitié-Salpêtrière, 47 Boulevard de l'hôpital, 75013 Paris, France; [10]Centre de Référence de Pathologie Neuromusculaire Paris-Est, Institut de Myologie, GHU La Pitié-Salpêtrière, Assistance Publique-Hôpitaux de Paris, 7503 Paris, France; [11]Centre National de Génotypage, Institut de Génomique, CEA, CP5721, 91057 Evry, France; [12]Department of Radiology, Westmead Hospital, Western Clinical School, University of Sydney, Sydney, NSW 1024, Australia; [13]Department of Neurology, Concord Clinical School, University of Sydney, Sydney, NSW 2139, Australia; [14]Analytic and Translational Genetics Unit, Massachusetts General Hospital, Boston, MA 02114, USA; [15]Broad Institute of Harvard and Massachusetts Institute of Technology, Cambridge, MA 02142, USA; [16]Service de Biochimie et Génétique Moléculaire, HUPC Hôpital Cochin, Paris 75014, France; [17]INSERM, U1016, Institut Cochin, CNRS UMR8104, Université Paris Descartes, Paris 75014, France; [18]Electron Microscope Unit, Concord Repatriation General Hospital, Concord, NSW 2139, Australia; [19]The Clive and Vera Ramaciotti Centre for Structural Cryo-Electron Microscopy, Monash University, Melbourne, VIC 3800, Australia; [20]Department of Biochemistry and Molecular Biology, Monash University, Melbourne, VIC 3800, Australia; [21]Department of Pediatric Neurology, Hacettepe University Children's Hospital, 06100 Ankara, Turkey; [22]Centre for Medical Research, The University of Western Australia & the Harry Perkins Institute of Medical Research, Perth, WA 6009, Australia; [23]Murdoch Children's Research Institute, The Royal Children's Hospital, Flemington Road, Parkville, VIC 3052, Australia; [24]Université de Strasbourg, 67081 Illkirch, France
[25]These authors contributed equally to this work
[26]These authors contributed equally to this work
[27]These authors contributed equally to this work
*Correspondence: sandra.cooper@sydney.edu.au
http://dx.doi.org/10.1016/j.ajhg.2016.09.005.

patients,[2,3] driving ongoing gene discovery. The introduction of next-generation sequencing technologies has seen a rapid acceleration in the identification of new genetic causes of neuromuscular disorders.[4,5]

Through international whole-exome sequencing programs in Australia, France, the United States, and Turkey, we identified five families (nine probands) with four different recessive variants (missense and splicing variants) in *PYROXD1*. *PYROXD1* is located at 12p12.1 and encodes pyridine nucleotide-disulfide oxidoreductase domain-containing protein 1, a 500 amino acid protein previously undescribed in published literature. Pyridine nucleotide-disulphide reductases (PNDRs) are flavoproteins (FAD-binding) and catalyze the pyridine nucleotide (NAD/NADH)-dependent reduction of cysteine residues in their substrates.[6] PNDRs catalyze complex reduction reactions and use several steps of electron transfer via their enzymatic co-factors FAD and NAD. Although functionally uncharacterized, PYROXD1 is classified as a class 1 oxidoreductase and bears two putative enzymatic domains: a pyridine nucleotide-disulphide oxidoreductase domain (amino acids 39–361) and a NADH-dependent nitrite reductase domain (amino acids 447–494) (see Figure 3).

Herein we establish PYROXD1 as a nuclear-cytoplasmic oxidoreductase that underlies an early-onset myopathy characterized by generalized weakness with multiple internalized nuclei and myofibrillar aggregates on biopsy.

Subjects and Methods

Genetic Analysis

Family A was the index family identified through whole-exome sequencing of a large cohort of undiagnosed myopathy and dystrophy patients (367 individuals from 193 families) recruited from The Institute for Neuroscience and Muscle Research (Sydney, Australia). No further families were identified in this cohort with PYROXD1-related disease. Exome sequencing was performed on gDNA from both brothers and their unaffected parents at the Broad Institute using the XBrowse bioinformatics platform as described previously.[7] Family B was identified through the French Myocapture project (1,000 exomes from 397 families with myopathies or dystrophies). Exome sequencing was performed for both affected brothers and their parents at Centre National de Génotypage (CNG, Evry, France). Common variants (>1%) found in dbSNP, 1000 Genomes, Exome Variant Server, and an internal database of 1,550 exomes including ethnically matched individuals were filtered out. The Varank pipeline was used for variants scoring and ranking.[8] Data were filtered for homozygous recessive variants based on the known consanguinity of the family. Family B was the only family identified with recessive *PYROXD1* variants in the Myocapture cohort. For family C, exome sequencing was performed through the NIH Intramural Sequencing Center (NISC) on genomic DNA obtained from both affected siblings. Data were analyzed using a custom analysis program, MPG (Most Probable Genotype) based on a probabilistic Bayesian algorithm.[9] For families D and E, exome sequencing was performed on gDNA from both siblings and unaffected parents at the Theragen Etex Bio Institute. ANNOVAR was used to functionally annotate genetic variants.[10] Table S1 provides a list of recessive variants shown to segregate with disease for each family.

Phylogenetic Analysis and Calculation of the PYROXD1 Homology Model

PYROXD1 sequence alignments were performed using CLUSTAL.[11] Identity and similarity were calculated using Sequence Manipulation Suite.[12,13] Modeler[14] was used to compare the primary sequence of PYROXD1 with homologous proteins in the PDB database. The primary sequence of PYROXD1 was aligned with eight of the most similar protein sequences determined from Modeler using Promals3D:[15] *Shewanella* PV-4 NADH-dependent persulfide reductase (PDB: 3NTD), *Staphylococcus* Coenzyme A-disulfide reductase (PDB: 1YQZ), *Bacillus* Coenzyme A-disulfide reductase (PDB: 3CGC), *Novosphingobium* ferredoxin reductase (PDB: 3LXD), *Rhodopseudomonas* ferredoxin reductase (PDB: 3FG2), *Pseudomonas p.* putidaredoxin reductase (PDB: 1Q1R), *Pseudomonas sp.* ferredoxin reductase (PDB: 2GQW), and *Enterococcus* NADH peroxidase (PDB: 1NHQ). Modeler was used to compute the homology model of human PYROXD1 using information from all eight homologous crystal structures. The resulting model with the lowest energy was further refined using Modrefiner.[16] FAD binding residues were determined via the 3DLigandSite server.[17] Figures were generated with Pymol (The PyMOL Molecular Graphics System, v.1.8, Schrödinger, LLC).

Western Blot

Western blot of skeletal muscle and skin fibroblasts was carried out as described in Yuen et al.[18] Primary antibodies used were anti-PYROXD1 (1:1,000; Abcam cat# ab122458; RRID: AB_11129858), β-tubulin (1:1,000; E7, Developmental Studies Hybridoma bank), GAPDH (1:10,000; Millipore cat# MAB374; RRID: AB_2107445), Emerin (NCL 1:300, Novocastra), and sarcomeric alpha-actinin (EA-53 1:2,500, Sigma-Aldrich). For zebrafish, embryos were deyolked and protein extracted as described.[19] 13 μL of protein sample was reduced using NuPAGE Reducing Agent (Thermo Fisher) and equal amounts loaded onto a NuPAGE 4%–12% Bis-Tris Gel using MES SDS running buffer (Thermo Fisher). Membranes were blocked and probed with antibodies diluted in 1× phosphate-buffered saline, 0.1% Tween20 (Sigma-Aldrich), and 5% skim milk. Primary antibodies used were 1:1,000 anti-Ryroxd1-C (Abmart), 1:1,000 anti-GFP (Abcam cat# ab137827), and 1:2,000 α-tubulin (Sigma-Aldrich cat# T6074; RRID: AB_477582). The secondary antibody used was 1:10,000 HRP-conjugated mouse IgG (Southern Biotech) and developed using chemiluminescent detection (GE Life Sciences). For yeast, total yeast extracts were obtained by NaOH lysis followed by TCA precipitation. The equivalent of 1.5 OD_{600nm} unit of yeast cells were resuspended in 50 μL of 2× Laemmli buffer plus Tris Base. Samples were incubated 5 min at 37°C and analyzed by 10% SDS-PAGE followed by immunoblotting with anti-PYROXD1 (1:500), polyclonal R3500 produced in rabbit with human PYROXD1 immunogen amino acid 488–500 (Cys Leu Leu Asp Pro Asn Ile Asp Ile Glu Asp Tyr Phe Asp). Images were acquired with the ChemiDoc Touch Imaging System (Bio-Rad).

Immunostaining and Microscopy

For skeletal muscle, 8 μm muscle cryosections were fixed in 3% paraformaldehyde for 15 min, extracted with cold methanol for

10 min, and probed with primary antibodies diluted in 2% BSA/PBS for 16 hr at 4°C: PYROXD1 (1:50; Abcam cat# ab122458 or ab204560; RRID: AB_11129858), desmin (1:50; NCL-Des, Novacastra), myosin (1:20; RS034, Novacastra), and lamin A/C (1:80; NCL-LAM-A/C, Novacastra). After washing in PBS, samples were incubated with secondary antibody for 1 hr at room temperature, washed, and mounted with ProLong Gold with DAPI antifade reagent (Life Technologies). Goat anti-rabbit $IgG^{Alexa555}$ goat anti-mouse $IgG^{Alexa488}$ (H+L) (1:200, A21428 and A110018, Life Technologies). Specimens were imaged on a Leica SP5 confocal microscope. For zebrafish, 4% paraformaldehyde (PFA)-fixed 2 dpf whole-mount or 4 dpf whole-mount and vibratome-sectioned embryos were stained as described.[19] Antibodies used were α-actinin2 (Sigma clone A7811, 1:100) and an AlexaFluor-labeled-488 secondary antibody (Molecular Probes, 1:200) and rhodamine-Phalloidin (Molecular Probes, 1:200). Imaging was performed with an LSM 710 confocal microscope (Zeiss), using a 20× 1.0 numerical aperture water-dipping objective.

For yeast, living cells expressing EGFP C-terminal-tagged PYROXD1, PYROXD1-Asn155Ser, or -Gln372His were imaged on a fluorescence Axio Observer D1 microscope (Zeiss) using GFP filter and DIC optics with 100×/1.45 oil objective (Zeiss). Images were captured with a CoolSnap HQ2 photometrix camera (Roper Scientific).

Cell Culture, Constructs, cDNA Synthesis, and Transfections

HEK293 cells were cultured and transfected as described.[20] Cos-7 cells and primary human fibroblasts were cultured in DMEM/F12 with 10% FBS and 1:200 gentamycin (all from Life Technologies). Cos7 cells were transfected with Lipofectamine LTX (15338-100, Life Technologies) as per the manufacturer's instructions in 10 cm^2 dishes. Human *PYROXD1* cDNA (GenBank: NM_024854) was cloned into pEGFP-CI (Genscript) via BspE1/Sal1. GFP was then removed via AgeI/BspEI. RNA extraction of primary human fibroblasts was carried out using TRIzol (Invitrogen) and alcohol precipitation. cDNA was synthesized using random primers $p(dn)_6$ (Roche 11043921) or $Oligo(dt)_{20}$ primers (Invitrogen 55063) and Superscript III reverse transcriptase (Invitrogen 56575) according to the manufacturer's instructions. Primers used for PCR of *PYROXD1* cDNA were exon 1 F: 5′-AGGGAAGTTCGTGGTGGTC-3′; exon 6 R: 5′-TGGCCCAAATCACTTCACAG-3′; exon 12 R: 5′-AGGACGAGAATACATCAAAGTCG-3′.

Plasmids, Strains, Media, and Methods for Yeast Cells

The PYROXD1 and missense mutants p.Asn155Ser or p.Gln372His cDNA sequences were cloned into pDONR221 entry vector (Invitrogen) and then into yeast destination vectors (Addgene) via the Gateway (Invitrogen) method to obtain the pAG415-promGPD-PYROXD1, p.Asn155Ser or p.Gln372His (pSF371 to pSF373) and pAG415-promGPD-PYROXD1-EGFP, p.Asn155Ser or p.Gln372His (pSF374 to pSF376) plasmids. Plasmid sequences were verified (GATC Biotech). *S. cerevisiae* strains used were BY4742 WT (*MATα leu2Δ0 ura3Δ0 his3Δ0 lys2Δ0*) and *glr1Δ* (BY4742 *glr1:kanMX*). Yeast were grown in YPD-rich medium (1% yeast extract, 2% peptone, 2% glucose) or in Synthetic Medium (SD): 0.67% yeast nitrogen base (YNB) without amino acids, 2% glucose, and the appropriate –Leu dropout mix to maintain the plasmid. Yeast cells were transformed using the modified lithium acetate method.[21]

Zebrafish

Production of Transgenic Constructs, Morpholino Injections, and RNA Rescue Experiments

Zebrafish were maintained according to standard protocols.[22] Transgenic constructs were assembled with the modular tol2 kit. N-terminal eGFP-tagged wild-type or mutant PYROXD1 constructs were created using p5E-actc1b,[23] p5E-SP6-CMV,[24] p3E-pA, and pDEST-Tol2-pA2. Transgenic constructs used were actc1b-h2afv-mCherry[24] and actc1b-actinin3-mCherry.[25] For morpholino injections, ryroxd1 morpholinos (splice MO: 5′-TCGATGGTTTCTTACCTGTTCTGCA-3′, 0.25 mM and ATG MO: 5′-CCATTGAACTTCAGCACATGGAGAT-3′, 0.25 mM) and GFP morpholino (5′-GTTCTTCTCCTTTACTCAGGATC-3′, 0.5 mM) were diluted in distilled water and co-injected with Cascade Blue-labeled dextran (Molecular Probes) into one-cell embryos. For RNA rescue experiments, wild-type PYROXD1-eGFP RNA, lacking the morpholino binding site, was synthesized using the mMessage mMachine SP6 Transcription Kit (Ambion). RNA was co-injected at a concentration of either 0.5 or 1 ng/μL into one-cell stage embryos with Cascade Blue. Injected embryos were sorted for Cascade Blue labeling prior to analysis.

In Situ Hybridization

Whole-mount in situ hybridization was carried out as described previously.[26] Probes were constructed using specific gene primers (F: 5′-AGAAACCGAAGATGGTCAGAGA-3′ and R: 5′-GAGCGAAGACGCTTCTCTTCTA-3′). Imaging was performed with an Olympus SZX16 stereomicroscope.

cDNA Synthesis and Quantitative PCR

Total RNA was extracted using TRIzol reagent (Invitrogen Life Technologies) and cDNA was synthesized using Protoscript first strand cDNA synthesis kit (New England Biosciences). Quantitative PCR (qPCR) was performed on a Roche Lightcycler instrument using β-actin as a reference gene. Primers for qPCR are β-actin (F: 5′-GCATTGCTGACCGTATGCAG-3′ and R: 5′-GATCCACATCTGCTGGAAGGTGG-3′) and ryroxd1 (F: 5′-TCAATGGCTTCAGAGAAACAAG-3′ and R: 5′-CTGTTCTGCACAAGTGACACC-3′).

Swimming Assays

Touch-evoked response assays and analysis were performed on 48 hr post fertilization zebrafish as per Sztal et al.[19]

Electron Microscopy

Zebrafish were fixed in 2.5% gluteraldehyde, 2% paraformaldehyde in 0.1 M sodium cacodylate buffer, with post-fixation in 1% OsO_4 1.5% K3Fe(III)(CN)6 in 0.065 M sodium cacodylate buffer. Samples were dehydrated through an ethanol series and embedded in Epon 812. 80 nm sections were stained with Uranyl acetate and lead citrate before imaging using a Hitachi H-7500. Muscle biopsies were fixed in 2.5% glutaraldehyde in 0.1 M sodium cacodylate buffer and processed routinely for electron microscopy. Ultrathin sections were examined in an FEI Tecnai Spirit Biotwin.

Study Approval

Ethical approval for this research was obtained from the Human Research Ethics Committees of the Children's Hospital at Westmead, Australia (10/CHW/45), The University of Western Australia, the Comité de Protection des Personnes Est IV (DC-2012-1693), France, the Institutional Review Board of the National Institute of Neurological Disorders and Stroke, NIH (12-N-0095), and Ethical Committee of Hacettepe University, Faculty of Medicine. Written informed consent was obtained from participants for genetic testing, biobanking of DNA, muscle, and fibroblasts,

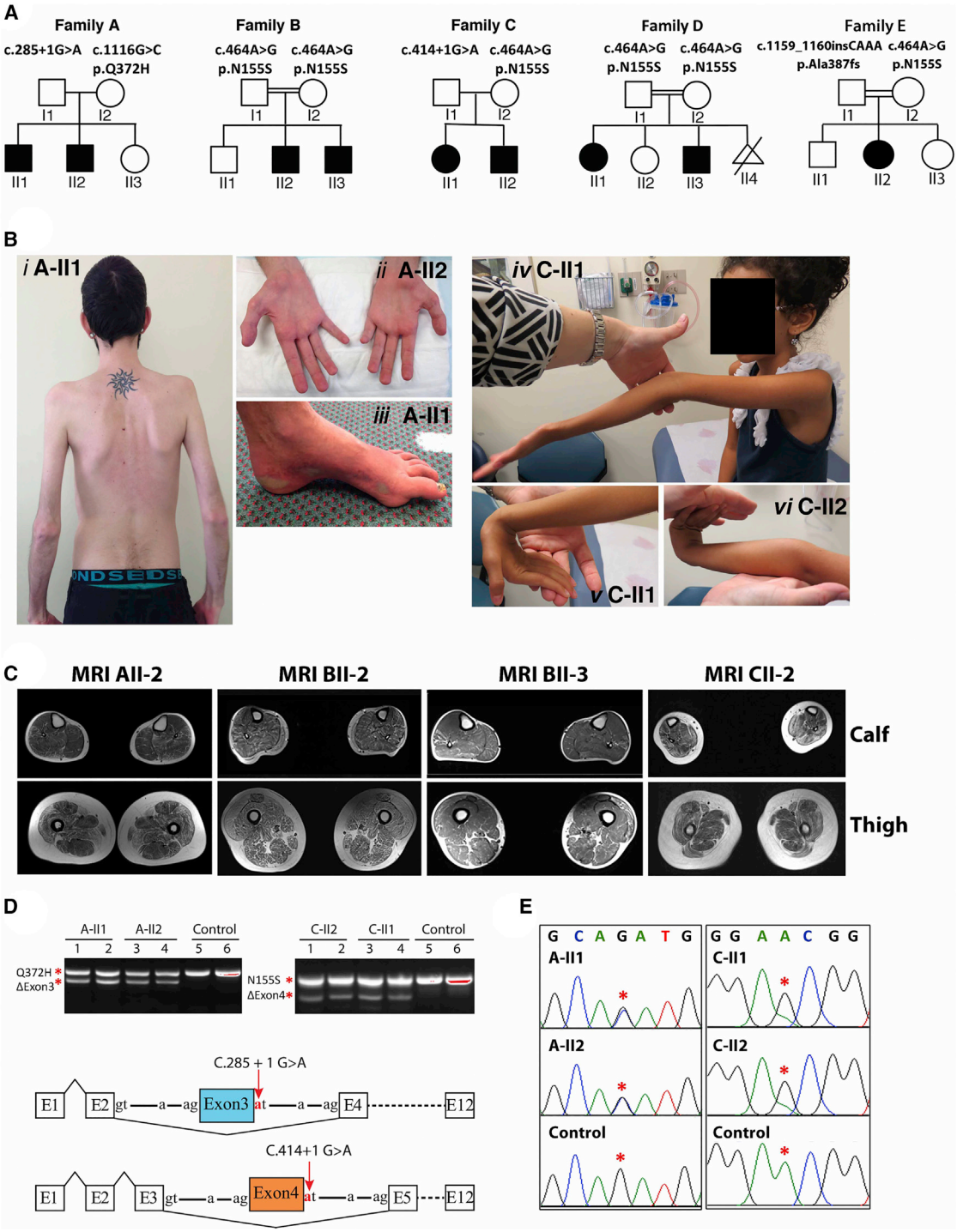

Figure 1. Clinical Features of *PYROXD1*-Related Myopathy

(A) Pedigrees of the five affected families.

(B) Posterior view of A-II1 (*i*) demonstrating generalized reduction of muscle bulk and prominent scapulae. Hands of A-II2 (*ii*) demonstrating marked wasting of the thenar and hypothenar eminence. Foot of A-II1 (*iii*) showing pes cavus and skin discoloration. C-II1 (*iv*) demonstrating hyperextension of the elbow and reduced muscle bulk. C-II1 (*v*) wrist hyperextension. C-II2 (*vi*) hand and wrist hyperextension.

(C) Axial T1 muscle MRI of calf and thigh of individuals A-II2, B-II2, B-II3, and C-II2. In all individuals, the thigh shows generalized reduction in muscle, atrophy, and fatty marbling. There is relative sparing of rectus femoris relative to vastus lateralis. The calf of individuals in family B is more mildly affected.

(D) Top: Agarose gel of PCR products of fibroblast cDNA from two affected siblings from family A (left) and family C (right). For both families, sequencing of the lower band established in-frame skipping of exon 3 in family A and exon 4 in family C. Sequencing of the upper band in family A identified only transcripts bearing the maternal c.1116 G>C (p.Gln372His) missense variant. Sequencing

(legend continued on next page)

and publishing of photographs of affected individuals. Fish maintenance and handling were carried out as per standard operating procedures approved by the Monash Animal Services Ethics Committee.

Results

Recessive *PYROXD1* Variants Cause Early-Onset Myopathy with Combined Histopathology of Multiple Internalized Nuclei and Myofibrillar Disorganization

Clinical Features of PYROXD1 Myopathy

Nine affected individuals from five families presented with childhood-onset muscle weakness (infancy to 8 years) (Figure 1A; Table 1). Perinatal history and early gross motor milestones were largely within normal limits. All affected individuals walked between 9 and 20 months of age. Two probands had poor head control in infancy (family C, II1 and II2). Weakness was slowly progressive. All affected individuals were still ambulant at 7–31 years but had difficulty with running and stairs. A-II1 required a cane for support and was unable to climb stairs from 24 years. All individuals had generalized reduction in muscle bulk (Figure 1B) and displayed symmetrical proximal weakness of the upper and lower limbs. Triceps brachii power was disproportionally reduced in three affected individuals. Distal weakness of the upper and lower limbs was also present in families A, B, C, and E. A-II1 and A-II2 showed marked wasting of distal musculature, in particular the thenar and hypothenar muscles (Figure 1B, *ii*), with abductor digiti minimi strength graded 3/5 and abductor pollicus brevis 0/5 in A-II2.

Neck weakness and mild scapular winging (5/9) were present (Figure 1B, *i*). Deep tendon reflexes were reduced or absent. Moderate joint laxity was present in families A and C (Figure 1B, *iv*–*vi*) but had resolved in family A by adulthood. Joint contractures did not occur, with the exception of mild tendoachilles contractures in A-II1. Mild scoliosis was seen in 2/9, pectus excavatum in 2/9, and thoracolumbar rigidity in family C. All affected individuals had mild to moderate facial weakness and mild ptosis was present in 3/9. A high arched palate and dental malocclusion were present in 7/9. Nasal speech was present in all individuals, swallowing difficulties in 6/9, fatigue with chewing in 2/9, and A-II2 required surgery for velopharyngeal incompetence. Ophthalmoplegia was not present.

Cognition was normal, except A-II1 who had mild, specific learning difficulties. Mild restrictive lung disease was present in the teenage years, but no individual had nocturnal hypoventilation. Frequent respiratory infections were seen in 4/9. Cardiac evaluations were normal, except for A-II1 who had developed abnormal septal wall motion and a low normal ejection fraction (50%) on his most recent assessment at 27 years of age.

Creatine kinase levels ranged from normal to moderately elevated (up to 1,051 IU/L). Electromyography (EMG) was myopathic in all individuals tested. Electrophysiological studies are summarized in Table S2. Nerve conduction studies in A-II1 and A-II2, the oldest affected individuals (26 and 29 years of age), found compound muscle action potential (CMAP) amplitudes reduced to 1%–10% of normal, absent peroneal CMAPs, reduced sural sensory potentials, but normal upper limb sensory amplitudes, suggestive of a mild length-dependent axonal neuropathy. Muscle MRI imaging of family A showed diffuse muscle atrophy and fatty marbling with relative sparing of rectus femoris relative to vastus lateralis in the thigh. In family B, only mild changes were seen, with vastus lateralis most affected in the upper leg and gastrocnemius in the lower leg (Figure 1C).

Histopathological Features of PYROXD1 Myopathy

Muscle biopsies were available from five affected individuals (Table 1). Haemotoxylin and eosin staining showed marked variation in fiber size and multiple internalized nuclei, commonly occurring in clusters (Figure 2A, *i*, *v*, *ix*, and see EM in Figure 2B, *i* and *vi*). Occasional degenerating and regenerating fibers were seen, with a moderate increase in interstitial connective tissue. Oxidative stains showed large central core-like zones devoid of mitochondrial activity (Figure 2A, *ii*, *vi*, *x* NADH). Immunohistochemical staining of skeletal muscle demonstrated large myofibrillar inclusions positive for desmin (Figure 2A, *iii*, *vii*, and *xi*), myotilin (Figure 2A, *iv* and *viii*), alpha-actin (Figure 2A, *xii*), and αB crystallin (not shown). Electron microscopy showed extensive sarcomeric disorganization, with small atrophied fibers showing complete loss of sarcomeric architecture, absence of aligned thick filaments, and accumulation of thin filaments (Figure 2B, *i*, *iii*, *iv*, *vi*, *vii*, *viii*). In some small fibers, electron-dense thickened z-line remnants or small nemaline rods were also present (Figure 2B, *iv* and *vii*). Large fibers showed multiple areas of Z-band streaming and large, focal zones of sarcomeric disorganization (Figure 2B, *ii*), devoid of mitochondria and organelles (Figure 2B, *v*). Thus, PYROXD1 myopathy

of the upper band in family C identified only transcripts bearing the maternal c.464A>G (p.Asn155Ser) variant. Bottom: Schematic of *PYROXD1* exon skipping events in family A and family C (not to scale).
(E) Sequencing chromatogram of the total PCR mixture using exon 1 forward and exon 12 reverse primers. Family A shows equal peak heights for the paternal wild-type and maternal missense variant c.1116 G>C (p.Gln372His) (red asterisks), suggesting approximately equal abundance of exon 3 skipped transcripts and missense c.1116 G>C (p.Gln372His) transcripts among the total mRNA pool. In contrast, family C shows evidence for maternal allele bias, with a lower peak height of the paternal c.464A relative to maternal c.464G variant (red asterisks).
Collective data (D, right and E, right) suggest that the paternal exon 4-skipped transcripts are less abundant than the maternal c.464A>G (p.Asn155Ser) among the total mRNA pool.

Table 1. Clinical Characteristics of Affected Individuals with PYROXD1 Variants

ID	Family A-II1	Family A-II2	Family B-II2	Family B-II3	Family C-II1	Family C-II2	Family D-II1	Family D-II3	Family E-II2
Gender, current age	male, 29 y	male, 26 y	male, 31 y	male, 21 y	female, 9 y	male, 7 y	female, 22 y	male, 17 y	female, 15 y
Ethnicity; consanguinity	European descent; no	European descent; no	Turkish; yes	Turkish; yes	Persian Jewish; no	Persian Jewish; no	Turkish; yes	Turkish; yes	Turkish; yes
PYROXD1 variants	c.285+1G>A (chr12: g.21598401G>A), c.116G>C (p.Gln372His, chr12: g.21615796G>C)	c.285+1G>A (chr12: g.21598401G>A), c. 0.116G>C (p.Gln372His, chr12: g.21615796G>C)	Hom. c.464A>G (p.Asn155Ser, chr12: g.21605064A>G)	Hom. c.464A>G (p.Asn155Ser, chr12: g.21605064A>G)	c.414+1G>A (chr12: g.21602626G>A), c.464A>G (p.Asn155Ser, chr12: g.21605064A>G)	c.414+1G>A (chr12: g.21602626G>A), c.464A>G (p.Asn155Ser, chr12: g.21605064A>G)	Hom. c.464A>G (p.Asn155Ser, chr12: g.21605064A>G)	Hom. c.464A>G (p.Asn155Ser, chr12: g.21605064A>G)	c.464A>G (p.Asn155Ser, chr12: g.21605064A>G), c.1159_1160insCAAA, chr12: g.21620457_21620458insCAAA)
Onset/progression	onset 5 y, difficulty running; slowly progressive weakness from 20 y; unable to climb stairs from 24 y; slow walk with a cane	onset 8 y; stable in childhood; mild progression from teenage years; increasing difficulty with stairs	onset 10 y; ambulant with difficulty ascending stairs	onset 10 y; ambulant	congenital onset; hypotonia; mild gross motor delay; walked age 20 mo; weakness from 6 y; increasing difficulty with stairs	infantile onset with hypotonia; walked age 13 mo; stable strength; difficulty with stairs	onset 2 y; ambulant; difficulty running and climbing; frequent falls; slowly progressive weakness from 20 y	onset 2.5 y; ambulant; difficulty climbing; stable in childhood	onset 4 y; easy fatigue; frequent falls; difficulty on stairs; slowly progressive; increasing difficulty with stairs
Pattern of limb weakness (HP:0001324)	symmetrical; UL, LL, axial; P, D	symmetrical; UL, LL, axial; P, D	symmetrical; UL, LL, axial; P UL, D LL	symmetrical; UL, LL, axial; P	symmetrical; UL, LL, axial	symmetrical; UL, LL, axial	symmetrical; UL, LL, axial; P	symmetrical; UL, LL, axial; P	symmetrical: UL, LL; P, D
Severity of limb weakness	all 4− and 4/5, except deltoid 2/5, shoulder abduction 1/5	all 4+ and 5/5, except deltoid 2/5, ADM 3/5, APB 0/5; lower limbs 4/5 except hip flex 3/5	–	–	all 4+ and 4−/5, except shoulder abd. 3/5, wrist flex 3+/5, neck flex 2/5, hip abduction 3/5	all 4 and 4−/5, except deltoid 3+/5, finger spread 3+/5, neck flex 2/5; hip extension 5−/5	proximal 4−, distal 4+/5, lower limbs more affected	proximal 4+ and 5−/5, distal 5/5	proximal 4− and 4+/5; hip flexion 3/5; thenar wasting
Hyporeflexia (HP:0001265)	reduced or absent	reduced or absent	reduced or absent	reduced or absent	reduced or absent	reduced or absent	reduced or absent	reduced or absent	reduced or absent
Achilles contractures (HP:0001771)	yes	no	no	no	yes	no	no	no	no
Joint contracture 5th finger (HP:0009183)	yes	no	no	no	yes	no	no	no	no
Joint hypermobility (HP:0001382)	distal laxity, resolved with age	distal laxity, partial patella subluxations	no	no	elbow and MCP joints	mild at elbow, wrist, and MCP joints	no	no	no
Facial weakness (HP:0002058)	yes	yes	yes	yes	yes	yes	yes	yes	yes
Ptosis (HP:0000508)	no	no	no	mild	no	no	mild	mild	no

(*Continued on next page*)

Table 1. ***Continued***

ID	Family A-II1	Family A-II2	Family B-II2	Family B-II3	Family C-II1	Family C-II2	Family D-II1	Family D-II3	Family E-II2
Ophthalmoplegia (HP:0000602)	no	no	no	no	no	no	no	no	no
High arched palate (HP:0000218)	yes	yes	no	no	yes	yes	yes	yes	yes
Additional facial features	dental malocclusion (HP:0000689), elongated face	dental malocclusion (HP:0000689), elongated face	no	micrognathia and retrognathia (HP:0000308)	int. exotropia, surgical correction (HP:0000577)	no	elongated face (HP:0000276)	elongated face (HP:0000276)	no
Dysphagia (HP:0002015)	present from 12 y; improved	yes, plus nasal regurgitation from 9 y; surgery for VPI	yes	no	no	no	yes	yes	yes
Chewing difficulties (HP:0030193)	no	no	no	no	yes	yes	no	no	no
Nasal speech (HP:0001611)	yes	yes	yes	yes	yes	yes	yes	yes	yes
Scoliosis (HP:0002650)	mild thoracic scoliosis from 20 y	no	no	no	mild scoliosis from 7 y	no	no	no	no
Spinal rigidity (HP:0003306)	no	no	no	no	thoracolumbar rigidity	thoracolumbar rigidity	no	no	no
Pectus excavatum (HP:0000767)	yes	no	no	no	yes	no	no	no	no
Scapular winging (HP:0003691)	yes	no	mild	mild	mild	mild, asymmetric	no	no	no
Pes cavus (HP:0001761)	yes	no	no	no	no	no	no	no	no
Pes planus (HP:0001763)	no	yes	yes	yes	no	no	yes	yes	no
Restrictive lung disease (HP:0002091)	yes, from 15 y	no	no	yes	no	no	no	no	no
Recurrent infections (HP:0002783)	no	no	no	no	yes	yes	yes	no	yes
Cardiac disease	abnormal septal motion and low normal ejection fraction at 27 y	no	no	no	mild to moderate pulmonic insufficiency	no	no	no	mild mitral and tricuspid insufficiency (HP:0001653)
Elevated CK (IU/L) (HP:0040081)	no (148–262)	yes (118–1,051)	yes (500–700)	yes (700–800)	no	no	yes (400–700)	no (290–376)	no

(*Continued on next page*)

Table 1. *Continued*

ID	Family A-II1	Family A-II2	Family B-II2	Family B-II3	Family C-II1	Family C-II2	Family D-II1	Family D-II3	Family E-II2
Histology	11 y	not performed	not performed	16 y	not performed	4 y	not performed	13 y	10 y
Internalized nuclei	yes	–	–	yes	–	yes	–	yes (>50% of fibers)	yes
Central cores	yes	–	–	yes	–	yes	–	yes on NADH and SDH stains	yes
Myofibrillar inclusions[a]	yes	–	–	yes	–	yes	–	EM not performed	EM not performed
Sarcomeric disorganization	yes	–	–	yes	–	yes	–	–	–
Thin filament accumulations	yes	–	–	yes	–	–	–	–	–
Nemaline rods	yes	–	–	yes	–	–	–	–	–

Abbreviations are as follows: UL, upper limb; LL, lower limb; P, proximal; D, distal; ADM, abductor digiti minimi; APB, abductor pollicus brevis; MCP, metocarpophalyngeal; VPI, velopharyngeal insufficiency; CMAP, compound muscle action potential; EMG, electromyography; NCS, nerve conduction studies; NCV, nerve conduction velocity; y, year; mo, month.
[a]Myofibrillar inclusions were positive to desmin, myotilin, alpha-actin, and αB crystallin.

has a distinctive histopathology that combines features seen in central and minicore disease, centronuclear, myofibrillar, and nemaline myopathies.

Genetic Analyses

Exome sequencing in five unrelated families identified compound heterozygous variants in *PYROXD1* (GenBank: NM_024854.3) in families A, C, and E and the same homozygous recessive missense variant in consanguineous Turkish families B and D (Figures 1A and 3). Sanger sequencing confirmed all variants and familial segregation was consistent with autosomal-recessive inheritance. DNA was not available for D-II2 or D-II4.

In family A, a paternally inherited essential splice site variant, c.285+1G>A (chr12: g.21598401G>A), was identified. The variant is found at low frequency in the heterozygous state in the Exome Aggregation Consortium (ExAC) database (allele frequency 4.295×10^{-5}).[27] cDNA analysis performed on muscle from A-II1 (not shown) and fibroblasts from A-II1 and A-II2 (Figure 1D) confirmed disruption of the donor splice site, with in-frame skipping of exon 3 a common consequence of the splice variant (Figure 1D, left gel, approximately equal levels of normal splicing [upper band] and exon 3 skipping [lower band]). PCR using exon 1 forward and intron 3 reverse primers did not provide evidence for increased frequency of exon 3 extension in family A relative to control fibroblasts (not shown). A second maternally inherited missense variant, c.1116G>C (p.Gln372His; chr12: g.21615796G>C), was not found in the ExAC database.[27] In silico predictions support pathogenicity (PolyPhen-2 score 1.0 = probably damaging;[28] Provean score −4.68 = deleterious;[29] MutationTaster score 0.999 = disease causing[30]). c.1116 G>C is the terminal 3′ base of exon 10, but cDNA analyses revealed no obvious consequence for splicing (Figures 1D and 1E) and approximately equal levels of the c.1116 G>C (p.Gln372His) variant on cDNA (Figure 1E, family A; equal peak heights at position c.1116G>C are asterisked).

In families B and D, exome sequencing identified a homozygous missense variant c.464A>G (p.Asn155Ser; chr12: g.21605064A>G) in the affected siblings (B-II2 and B-II3 and D-II1 and D-II3, Figure 1A). The variant was found at very low frequency in the ExAC database and always in the heterozygous state (allele frequency 7.157×10^{-5}).[27] In silico predictions support pathogenicity (PolyPhen-2 score 1.0 = probably damaging;[28] SIFT score 0.74 = tolerated; Provean score −4.97 = deleterious;[29] MutationTaster score 0.999 = disease causing[30]).

Families C and E (Figure 1A) had compound heterozygous variants including the c.464A>G (p.Asn155Ser; chr12: g.21605064A>G) missense variant described in family B and D. In family C an essential splice site variant c.414+1G>A (chr12: g.21602626G>A) was paternally inherited. The c.414+1G>A variant is present in the heterozygous state at very low frequency in ExAC (allele frequency 4.295×10^{-5}).[27] The c.414+1G>A (chr12: g.21602626G>A) variant is predicted to disrupt the donor splice site of exon 4.[30] cDNA analysis on skin fibroblasts

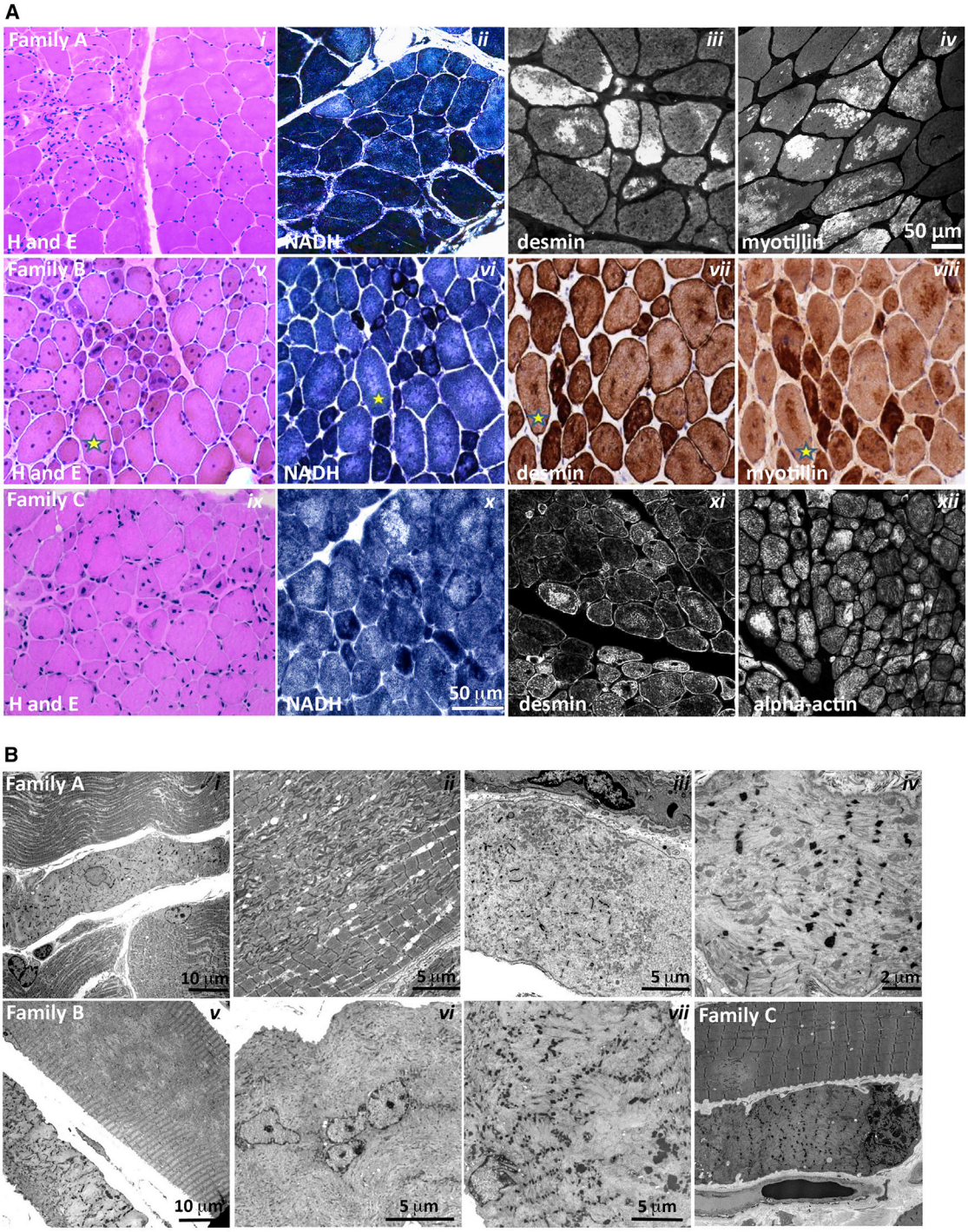

Figure 2. Histopathological Findings in PYROXD1 Myopathy

(A) Histopathological findings in skeletal muscle sections from family A (A-II1, quadriceps biopsy at 11 years of age), family B (B-II3, quadriceps biopsy at 16 years of age), and family C (C-II2, quadriceps biopsy at 4 years of age). Haemotoxylin and eosin (H&E) staining of muscle biopsy specimens from each family shows variation in fiber size, multiple internalized nuclei, and increased fibrous connective tissue. Immunofluorescent staining of skeletal muscle from A-II1 and C-II2 and immunoperoxidase staining from B-II3 demonstrate inclusions highly immunoreactive to desmin, myotillin, and alpha-actin (and αB-crystallin, not shown). H&E and immunoperoxidase images are provided via Hospital Pathology without a scale bar. Fibers in sequential sections of B-II3 are marked with a yellow star.

(B) Electron microscopy of muscle biopsy specimens. Family A: (*i*) small atrophic fiber with a central nucleus and loss of sarcomeric organization; (*ii*) large region of Z-band streaming with only occasional areas of normal sarcomeric register; and (*iii*, *iv*) atrophic fibers showing total loss of sarcomeric register, loss of thick filaments, and prominent Z-bands sometimes forming small nemaline bodies. Family B: (*v*) Large fibers show large central minicore-like regions devoid of normal myofibrillar structure and lacking mitochondria and organelles, with adjacent small fibers showing total loss of sarcomeric structure, accumulations of thin filaments, and loss of thick

(legend continued on next page)

from C-II1 and C-II2 confirmed that the c.414+1G>A splice site variant disrupts normal splicing, effecting in-frame skipping of exon 4 in a subset of transcripts (Figure 1D, right gel: normal splicing [upper gel], exon 4 skipping [lower gel]). PCR was also performed with exon 1 forward and intron 3 or intron 4 reverse primers. Family C fibroblast cDNA showed higher levels of exon 3 extension, relative to controls; no evidence for exon 4 extension was observed (not shown). Sanger sequencing of cDNA across the c.464A>G (chr12: g.21605064A>G) maternal variant showed some evidence for maternal allele bias (Figure 1E, family C, note lower peak height of the paternal c.464A relative to maternal c.464G variant, red asterisks). Collectively, our data suggest at least two outcomes from the c.414+1G>A donor splice variant; in-frame skipping of exon 4 and ectopic inclusion of intron 3 sequences that create a premature stop codon after 97 amino acids and may be subject to nonsense-mediated decay.

In family E the second variant was a heterozygous 4 bp insertion, c.1159_1160insCAAA (p.Ala387fs*13; chr12: g.21620457_21620458insCAAA), which was paternally inherited. This frameshift variant will encode a truncated protein lacking the conserved NADH-nitrile reductase domain and bearing 13 ectopic amino acids downstream of Ala387 before an early termination codon.

Families B, D, and E are Turkish. SNP markers in the region of the c.464A>G (chr12: g.21605064A>G) variant are consistent with a shared minimal confirmed haplotype between the three families of at least 348 Kb, from chr12: 21,331,987 to 21,680,609 (Table S3).

PYROXD1 Belongs to an Ancient Family of Oxidoreductases

PYROXD1 (pyridine nucleotide-disulphide oxidoreductase [PNDR] domain-containing protein 1) is classified as a class I pyridine nucleotide-disulphide oxidoreductase by neXtprot and UniProtKB. PNDRs are an ancient family of enzymes that regulate the redox state of other proteins. Unlike the five other human class I PNDRs—dihydrolipoamide dehydrogenase (DLD [MIM: 238331]), glutathione reductase (GSR [MIM: 138300]), and thioredoxin reductases 1, 2, and 3 (TXNRD1 [MIM: 601112], TXNRD2 [MIM: 606448], TXNRD3 [MIM: 606235])—PYROXD1 does not bear a consensus redox active site within the oxidoreductase domain (Gly Gly Thr Cys Val Asn Val Gly Cys in GSR and thioredoxin reductases, Gly Gly Thr Cys Leu Asn Val Gly Cys in DLD; reactive cysteine disulphide underlined). Moreover, PYROXD1 does not bear a conserved C-terminal dimerization domain identified in all other class I PNDRs, and instead bears a highly evolutionarily conserved nitrile reductase domain (69% identity and 85% similar in *Dictyostelium*). Though apparently divergent to other class I PNDRs, PYROXD1 is highly evolutionarily conserved, with 63% identity (78% similarity) of human PYROXD1 to zebrafish PYROXD1 and 39% identity (54% similarity) to *Dictyostelium* PYROXD1 (slime mold). Structural modeling of PYROXD1 using eight homologous solved crystal structures derived from other PNDRs support a predicted FAD-binding site (Figure 3B) that is vital for oxidoreductase activity of the PNDR family.[6]

The amino acids affected by the p.Gln372His and p.Asn155Ser substitutions are both highly evolutionarily conserved (Figure 3C), and removal of amino acids encoded by exon 3 (family A) or exon 4 (family C) (see Figures 3A and 3B) appears likely to significantly impact tertiary folding and abolish FAD binding and enzymatic function.

Missense Variants in Human PYROXD1 Impair Reductase Activity in Yeast

Redox activity of PYROXD1 was not previously reported, so we established a complementation assay in yeast to test the reductase activity of human PYROXD1 and the impact of identified missense variants. Replacing the yeast gene by its human counterpart is a powerful approach to help decipher the role of the human protein.[31,32] *Saccharomyces cerevisiae* has two overlapping oxidoreductase pathways, a cytoplasmic and a mitochondrial thioredoxin system, sharing some enzymes. To determine the localization of exogenous human PYROXD1 in yeast, GFP-tagged constructs were expressed in wild-type (WT) *S. cerevisiae* (Figure 3D). Fluorescent imaging of GFP-tagged PYROXD1 revealed widespread cytosolic localization, with wild-type, p.Asn155Ser, and p.Gln372His missense mutants showing similar, high expression in transformed *S. cerevisiae* by western blot (Figure 3F). Among the cytoplasmic yeast oxidoreductases, the Grl1 glutathione reductase localizes to the cytoplasm and mitochondria and is required for survival under oxidative stress.[33] Expression of non-tagged human PYROXD1 in *glr1Δ* mutant yeast that are hypersensitive to H_2O_2 due to lack of oxidoreductase activity rescued the growth defect of the *glr1Δ* mutant strain (Figure 3E), with wild-type and missense mutants showing similar, high protein levels in transformed *S. cerevisiae* by western blot (Figure 3F). Conversely, p.Asn155Ser and p.Gln372His PYROXD1 mutants failed to complement *glr1Δ* (Figure 3F). These data show that human PYROXD1 has a reductase activity that is strongly impaired by both identified missense variants.

Individuals with *PYROXD1* Variants Show Near-Normal or Reduced Levels of PYROXD1 Protein in Muscle, Fibroblasts, or Myoblasts

Western blot analysis of PYROXD1 protein levels showed a marked reduction in primary skin fibroblasts of A-II1 and

filaments; (*vi*) many large fibers have multiple internalized nuclei, often in clusters; and (*vii*) fibers show thin filament accumulations with electron-dense aggregates that resemble thickened z-lines and small nemaline bodies. Family C: (*viii*) Small atrophic fiber with loss of sarcomeric register. A large fiber shows multiple areas of Z-band streaming and a minicore-like region with absence of normal myofibrillar structure.

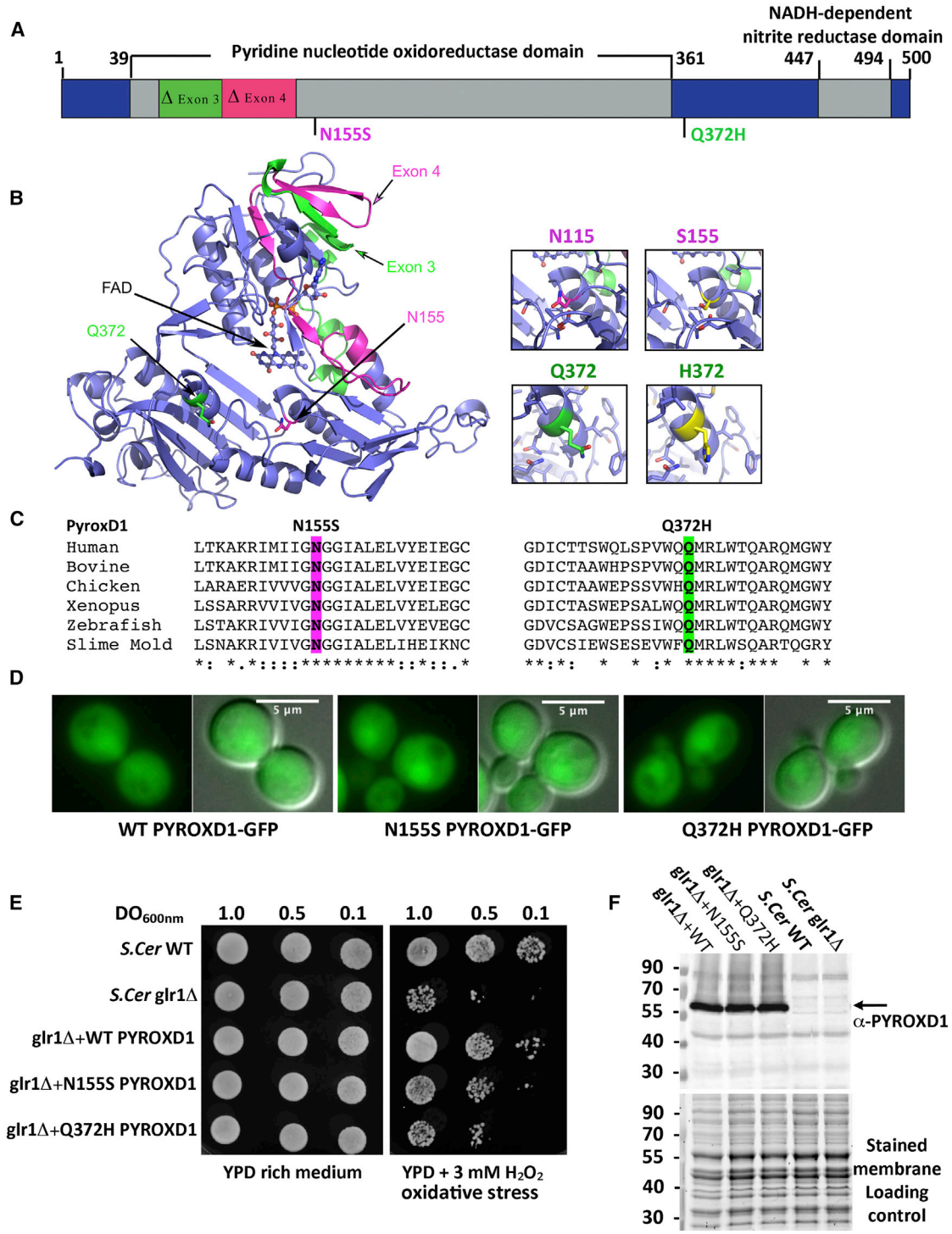

Figure 3. PYROXD1 Is an Oxidoreductase

(A) A schematic of PYROXD1 with functional domains and identified missense variants created using DOG 2.0.[35] Family A, Δexon3 and p.Gln372His (Q372H, green); families B and D, p.Asn155Ser (N155S); family C, Δexon4 and p.Asn155Ser (N155S, red).

(B) PYROXD1 homology model derived from eight homologous crystal structures (see Subjects and Methods). A co-ordinated FAD co-factor and the position of each identified variant on the crystal structure of PYROXD1 are highlighted in green (family A, Δexon3 and Q372H) and pink (family C: Δexon4 and N155S) as in (A).

(C) The identified missense variants p.Asn155Ser and p.Gln372His are evolutionarily conserved to primitive eukaryotes (Uniprot identifiers): human (Q8WU10), bovine (A7YVH9), chicken (F1NPI8), *Xenopus* (B1WAU8), *Danio rerio* (Q6PBT5), *Dictyostelium* (Q54H36).

(D) Living wild-type (WT, BY4742) yeast cells expressing human PYROXD1-GFP, PYROXD1-N155S-GFP, or PYROXD1-Q372H-GFP were observed by fluorescence microscopy with GFP filters and DIC optics. The merge represents the merge between the GFP and DIC images.

(legend continued on next page)

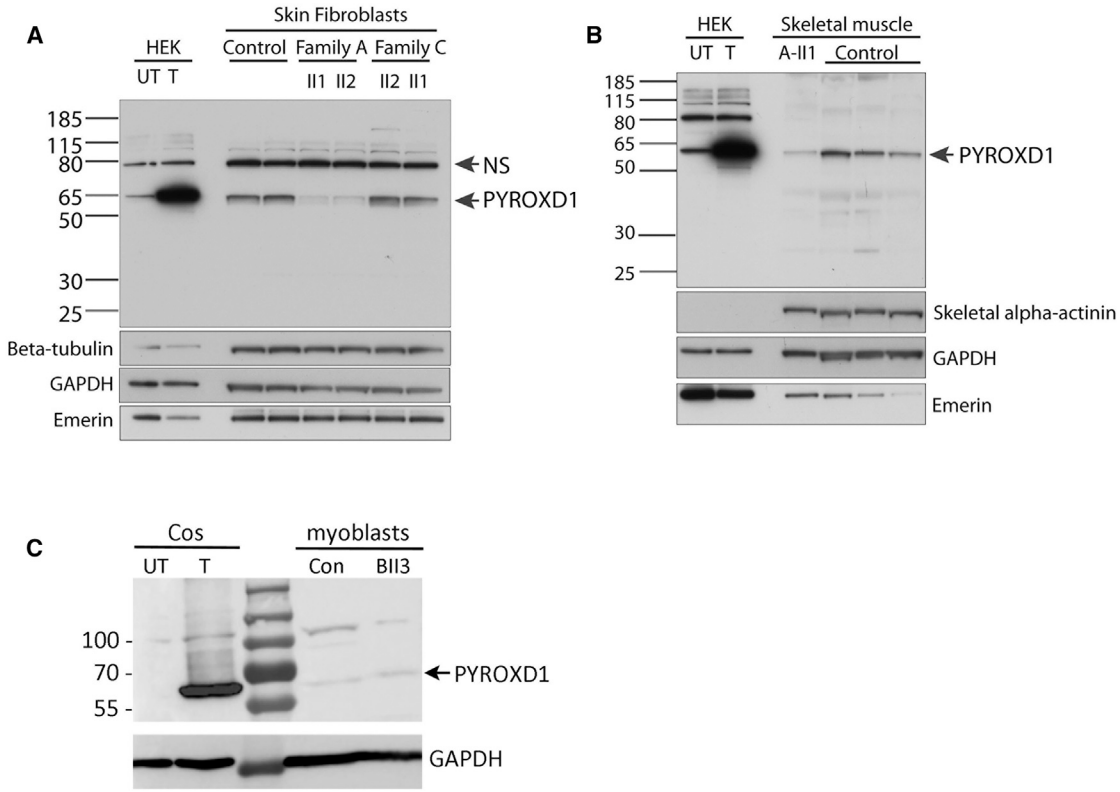

Figure 4. Affected Individuals with *PYROXD1* Variants Show Reduced or Near-Normal Levels of PYROXD1
(A) Western blot of skin fibroblasts from two controls (42 and 46 years of age) and affected siblings from family A (29 and 26 years) and family C (6 and 8 years). HEK293 cells transfected with a plasmid encoding human PYROXD1 establishes the apparent molecular weight of PYROXD1 at ~60 kDa (UT, untransfected; T, transfected). A non-specific (NS) band is indicated by an arrow. Levels of PYROXD1 are reduced in family A but not different to control levels in family C.
(B) Western blot of A-II1 triceps (11 years) (Abcam cat# ab122458; RRID: AB_11129858) shows reduced levels of PYROXD1 relative to three age-matched control biopsy specimens (quadriceps 11 years, 10 years, 15 years). Loading controls: β-tubulin and GAPDH control for overall protein content, with one cytoskeletal and one cytoplasmic marker; emerin controls for the number of nuclei; skeletal α-actinin controls for myofibrillar content.
(C) Western blot of myoblasts extracts from control subject and B-II3. Extracts from COS-1 cells transfected with the 500 aa human PYROXD1 cDNA (GenBank: NM_024854.3) was used as size control.

A-II2 (collected at 29 and 26 years of age) (Figure 4A, family A: ΔExon 3 and p.Gln372His), with no significant change in PYROXD1 levels in skin fibroblasts from C-II1 or C-II2 (8 and 6 years) (family C ΔExon 4 and p.Asn155Ser). In-frame deletion of exon 3 or exon 4 is predicted to remove 4.4 kDa or 4.7 kDa, respectively. Using two different anti-PYROXD1 antibodies (Abcam cat# ab122458 or ab204560; RRID: AB_11129858), we were unable to detect evidence for a lower molecular weight species, even with long exposures. Thus, our results suggest that in-frame deletions of exon 3 or exon 4 do not produce a stable protein. Western blot analyses of skeletal muscle specimens from A-II1 (collected at 11 years of age) similarly demonstrate reduced levels of PYROXD1 (Figure 4B), consistent with results in skin fibroblasts. Western blot analysis of family B (B-II3) cultured myoblasts detected low levels of PYROXD1 that did not appear altered compared to control (Figure 4C). Together, our data indicate that the splice variants lead to unstable proteins that are not detected by western blot, PYROXD1-Asn155Ser appears to have normal stability and protein levels (family B and C), whereas PYROXD1-Gln372His is detected at reduced levels (family A).

PYROXD1 Is a Nuclear-Cytoplasmic Oxidoreductase

Figure 5A demonstrates the localization of PYROXD1 in control human skeletal muscle longitudinal sections, lightly stretched (10% passive stretch) prior to fixation to facilitate resolution of thin and thick filaments. PYROXD1 protein shows a distinct nuclear localization and also

(E) Cultures of non-transformed wild-type (WT) or *glr1*Δ yeast, or *glr1*Δ yeast transformed with expression plasmids bearing wild-type, N155S-, or Q372H-PYROXD1 were spotted at the indicated concentration (OD_{600nm}) on rich (YPD) or on solid medium containing 3 mM H_2O_2. Plates were incubated at 30°C and observed after 48 hr.
(F) Western blot of non-transformed wild-type (WT) and *glr1*Δ, as well as *glr1*Δ yeast transformed with PYROXD1 expression vectors. The black arrow indicates PYROXD1 and the lower panel shows the protein-stained membrane used as loading control.

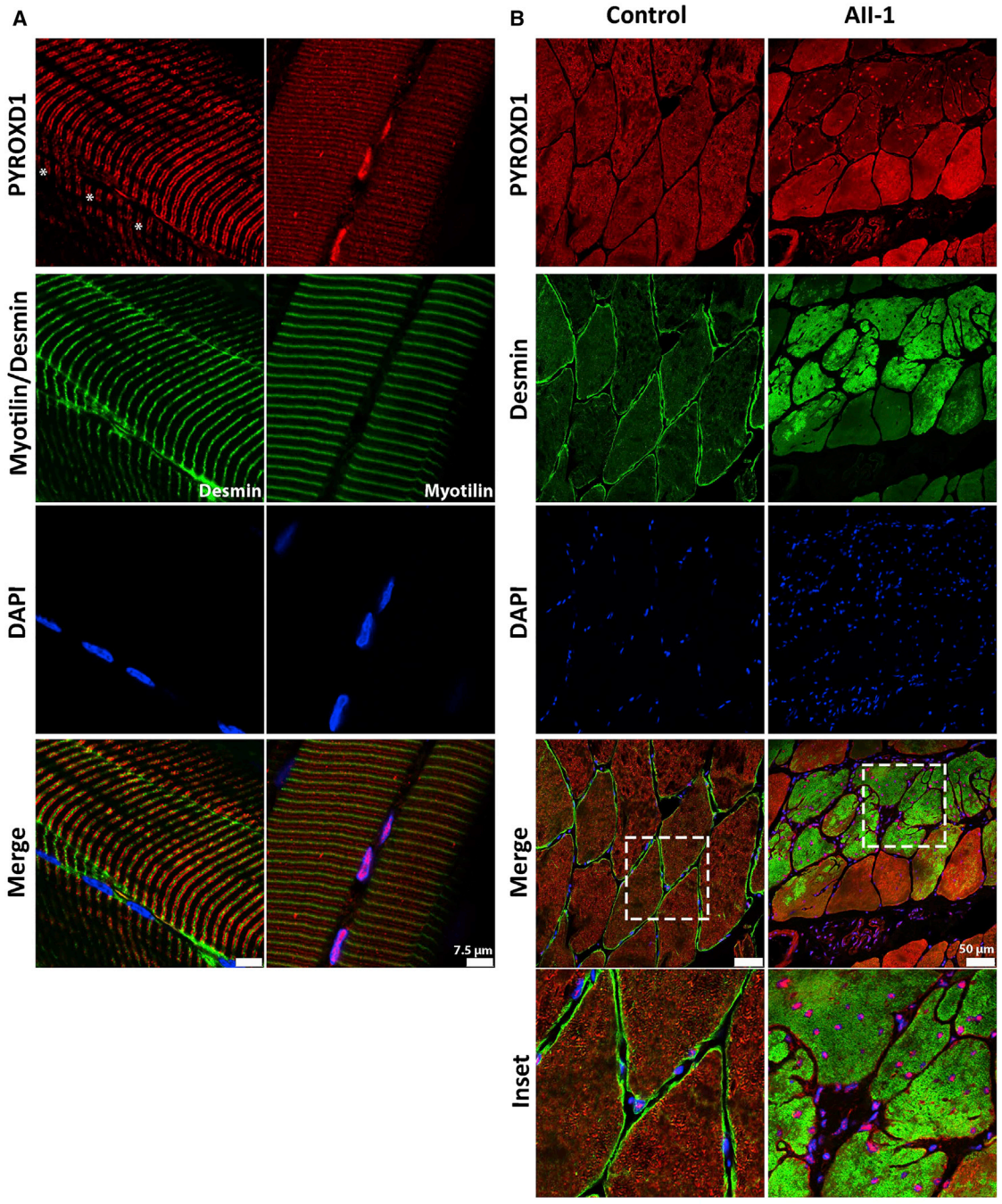

Figure 5. PYROXD1 Shows Both Nuclear and Striated Immunolocalization in Human Muscle
(A) Control stretched human skeletal (quadriceps) muscle co-stained with α-PYROXD1 (red), myotilin or desmin (green), and DAPI (blue). PYROXD1 intensely labels peripheral myonuclei, as well as showing two different patterns of striated labeling. Right: In this fiber, PYROXD1 brightly labels consecutive myonuclei and shows cytoplasmic striated labeling that aligns with desmin (Z-band region) and interdigitates between Z-bands (M-line region). Left: PYROXD1 does not brightly label myonuclei (asterisks show the position of DAPI-labeled nuclei) and shows a broader banding of striated labeling spanning the breadth of the I-band.
(B) Control and AII-1 tricep cross-sectioned human skeletal muscle co-stained with α-PYROXD1 (red), α-desmin (green), and DAPI (blue). The triceps muscle from AII-1 bears large inclusions that positively label for desmin, split fibers, and multiple internalized nuclei that brightly label for PYROXD1. Coverslips were imaged on a Leica SP5 confocal and single Z-planes are presented.

striated labeling (Figure 5A). PYROXD1 labels some peripheral nuclei more intensely than other nuclei (Figure 5A, left, asterisks show nuclei negative for PYROXD1). The sarcomeric compartment labeled by anti-PYROXD1 antibodies varied in different muscle specimens. Images presented show the two main types of striated labeling observed. The right panel of Figure 5A shows striations aligning both with the Z-band *and* interdigitating between Z-lines (near the M-band). The left panel shows a broader band of PYROXD1 labeling spanning the breadth of the

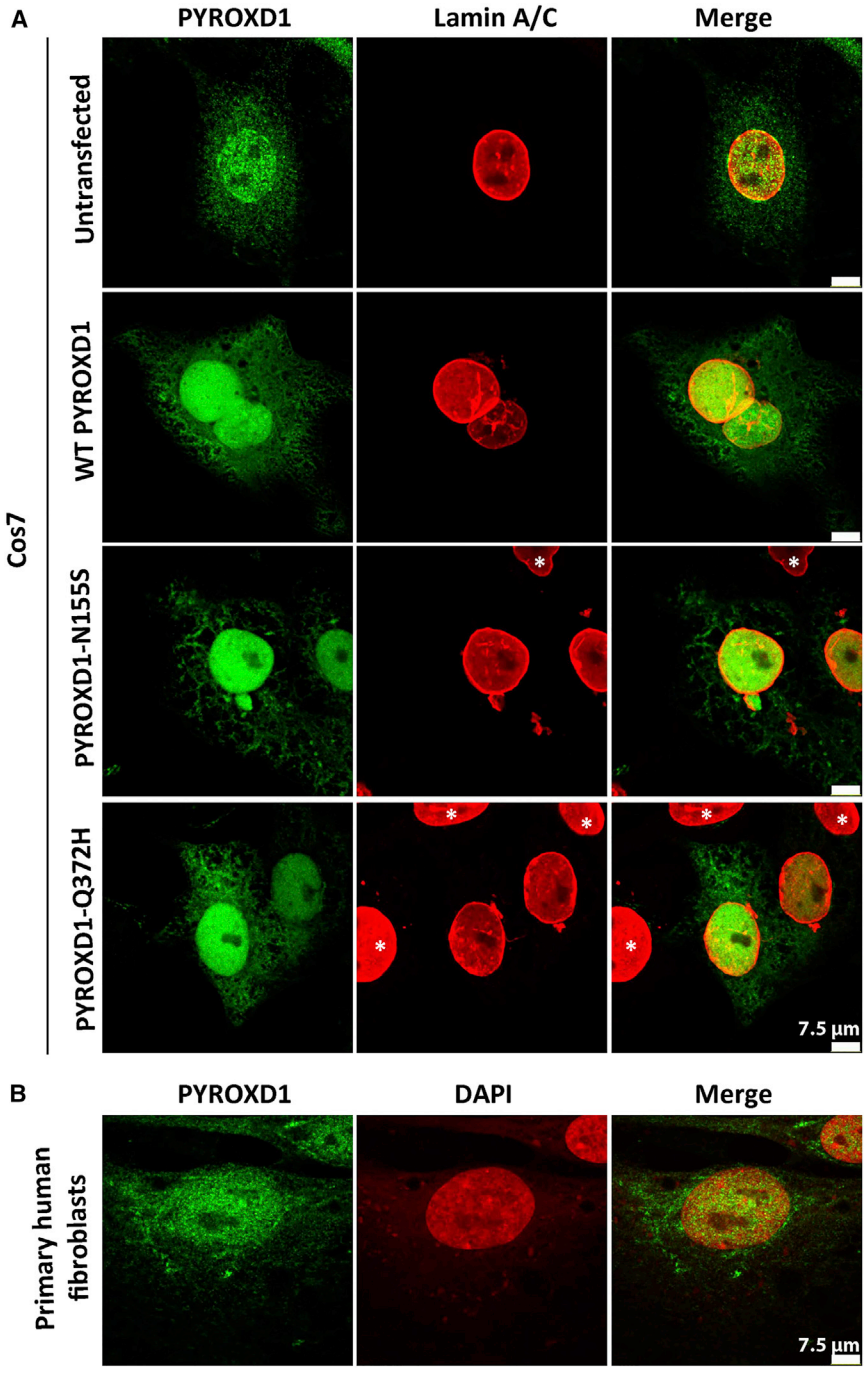

Figure 6. PYROXD1 Shows Nuclear Localization in Human Skin Fibroblasts and Transfected Cos-7 Cells

(A) Untransfected Cos-7 cells (top row) and Cos-7 cells transfected with human wild-type, p.Asn155Ser (N155S)-, or p.Gln372His (Q372H)-PYROXD1 expression constructs co-stained for PYROXD1 (green) and lamin A/C (red) shows enriched labeling for PYROXD1 within the nucleus, as well as labeling of cytoplasmic networks. For transfected Cos-7 cells (bottom three rows), asterisks demark untransfected cells within the field, with much lower levels of PyroxD1, that show very weak labeling under optimum capture conditions for transfected cells.

(B) Nuclear-cytoplasmic labeling is observed for endogenous PYROXD1 in primary human fibroblasts.

I-band. These data establish that PYROXD1 localizes to the nucleus and to sarcomeric/sarcoplasmic compartments.

Immunohistochemistry of control human skeletal muscle in cross section similarly shows dual localization of PYROXD1 in peripheral myonuclei as well as intramyofibrillar labeling throughout the contractile apparatus (Figure 5B). Levels of PYROXD1 in the triceps of A-II1 were lower relative to control muscle, and higher capture conditions are presented in order to portray key findings. As observed in the quadriceps of A-II1 (Figure 2A, *i*), the triceps muscle has large inclusions that label positively for desmin (Figure 5B, desmin, green) and multiple internalized nuclei (Figure 5B, DAPI, blue) that label positively for PYROXD1-Gln372His (Figure 5B, PYROXD1, red). Levels of cytoplasmic PYROXD1 appear brighter in myofibers *without* myofibrillar aggregates (Figure 5B, PYROXD1, red, enlarged inset). Thus, our results suggest that the equilibrium of cytoplasmic versus nuclear PYROXD1 is shifted to more predominant nuclear localization in muscle fibers burdened with myofibrillar aggregates.

Dual nuclear-cytoplasmic localization of PYROXD1 is supported by immunostaining of untransfected and transfected Cos-7 fibroblasts and primary human fibroblasts (Figure 6). Heterologous transfection of expression constructs encoding wild-type, p.Asn155Ser, or p.Gln372His PYROXD1 into Cos-7 fibroblasts showed a similar distribution of nuclear and cytoplasmic localization (Figure 6); similar patterns of staining for wild-type and PYROXD1 missense variants were also observed in transfected C2C12 myoblasts and immortalized human myoblasts (not shown). Moreover, no overt changes in PYROXD1 localization were observed in primary fibroblasts from two siblings from family A or two siblings from family C relative to fibroblasts from two age-matched controls (not shown).

PYROXD1 Shows Nuclear-Cytoplasmic Localization in Mature Zebrafish Myofibers, with Evidence for Aggregates Induced by Expression of p.Asn155Ser and p.Gln372His Mutant Constructs

To determine the localization of PYROXD1 within the skeletal muscle, we overexpressed eGFP-tagged wild-type and mutant (p.Asn155Ser and p.Gln372His) human PYROXD1 within zebrafish muscle using the muscle-specific *actc1b*

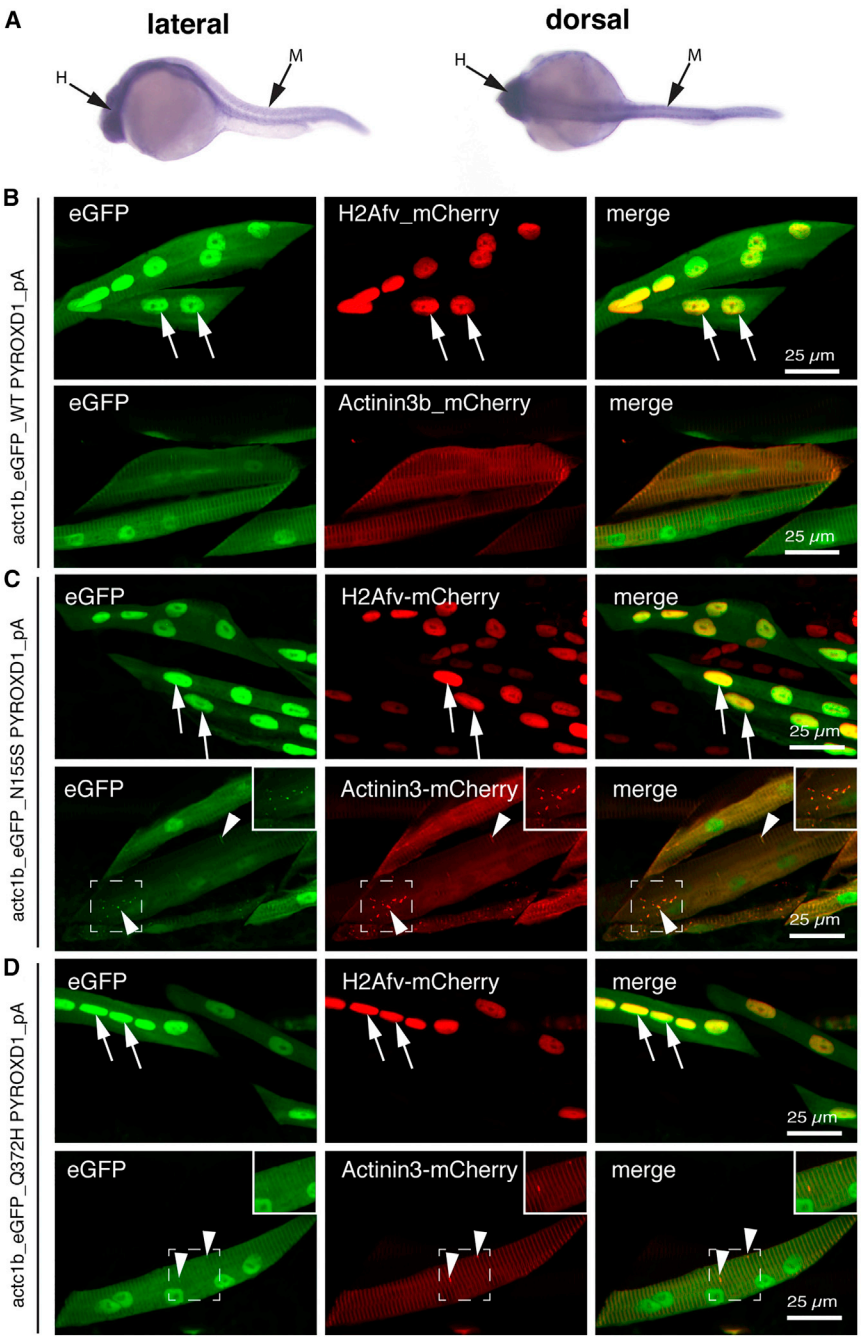

Figure 7. PYROXD1 Shows Nuclear-Cytoplasmic Localization in Zebrafish Myofibers, with Aggregates Induced by Expression of Asn155Ser and Gln372His Variants

(A) In situ hybridization on 24 hpf zebrafish shows widespread *ryroxd1* expression including the trunk musculature (M) in both lateral and dorsal views.

(B–D) Immunolabeling of vibratome-sectioned embryos 4 days post fertilization (dpf) expressing eGFP-conjugated human PYROXD1, either wild-type (B), p.Asn155Ser (C; N155S), or p.Gln372His (D; Q372H) via a muscle-specific actin promoter (*actc1b*) together with the Z-disk marker Actinin3-mCherry or nuclear marker histone H2A-mCherry. PYROXD1 localizes to myonuclei and shows striated labeling of sarcomeres. Small regions of thickening and sarcomeric disruption (arrowheads and inset) were observed after heterologous expression of N155S- or Q372H-PYROXD1, but not with wild-type PYROXD1.

promoter. All PYROXD1 constructs show dual nuclear and striated labeling aligning with the Z-disk, as evidenced by co-localization with actc1b:actinin3-mCherry and actc1b:H2Av-mCherry (Figure 7B, arrows). We also observed an occasional thickening of the Z-disk at 48 hpf when p.Asn155Ser and p.Gln372His PYROXD1 isoforms were overexpressed (Figures 7C and 7D, actinin3-mCherry arrowheads).

Zebrafish with Knockdown of RyroxD1 Show Sarcomeric Disorganization, Myofibrillar Aggregates, and a Defect in Swimming

We identified a single *PYROXD1* ortholog in zebrafish, *ryroxd1*, which is expressed throughout the developing embryo, including the skeletal muscle (Figure 7A). To study the function of Ryroxd1, we analyzed the effects of *ryroxd1* knockdown during early embryogenesis (Figure 8). Both quantitative PCR (qPCR) and western blot analyses confirm reduction of Ryroxd1 when *ryroxd1* ATG and exon2 splice morpholinos were used singularly and in combination (Figures 8A–8C).

To determine the effect of Ryroxd1 knockdown, we examined the swimming performance of the morpholino-injected embryos. Ryroxd1 single (ATG) and double (ATG and splice) morphants show a significant reduction in maximum acceleration in a touch-evoke response assay at 2 dpf compared to GFP morpholino-injected control zebrafish (Figure 8C). Co-injection of eGFP-tagged human wild-type PYROXD1 mRNA (wtPYROXD1-eGFP) with both Ryroxd1 morpholinos rescued the reduction in swim performance, demonstrating that the effect was due specifically to reduction of Ryroxd1 (Figure 9D).

Examination of zebrafish muscle through antibody labeling for Actinin2 and phalloidin shows no obvious defects in Ryroxd1 splice and ATG single morphants (Figure S1), but disrupted sarcomeric structure is evident in Ryroxd1 double morphants (Figure 8D). By 96 hpf, Actinin2 and phalloidin-positive aggregates are observed in Ryroxd1 ATG morphants (Figure S1). However, RyroxD1 double morphants show severe disruption of the musculature

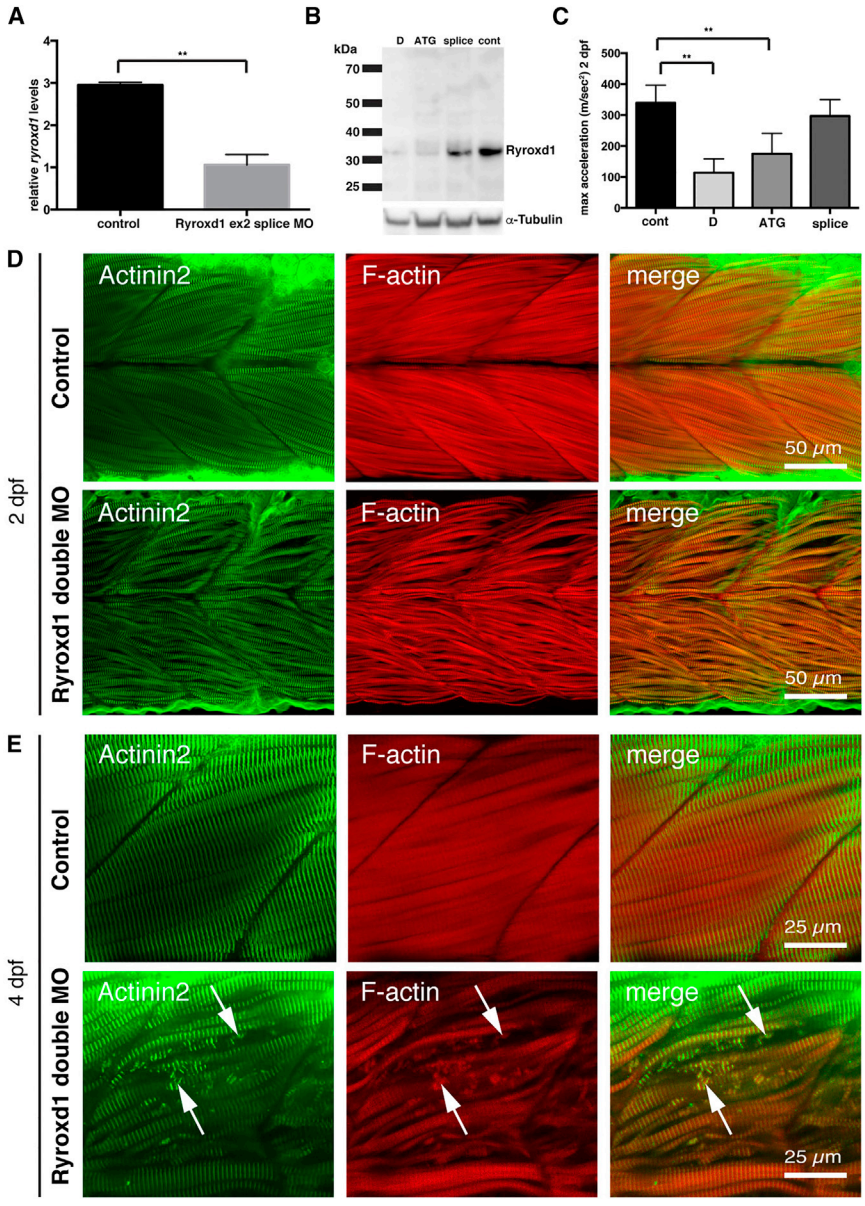

Figure 8. Zebrafish Deficient for RyroxD1 Show Sarcomeric Disorganization, Myofibrillar Aggregates, and a Defect in Swimming

(A) Quantitative PCR for *ryroxd1* mRNA levels in control (uninjected) and Ryroxd1 morpholino-injected (Ryroxd1 ex2 splice MO) zebrafish at 2 dpf.

(B) Western blot for Ryroxd1 protein and α-tubulin loading control in control (uninjected) and Ryroxd1 morpholino-injected zebrafish (D = Ryroxd1 double morpholino, ATG = Ryroxd1 ATG morpholino, and splice = Ryroxd1 splice-site targeting morpholino) at 48 hpf demonstrates effective reduction of Ryroxd1.

(C) Ryroxd1 ATG-single and ATG/splice double morphants show a significant reduction, of 48% and 73% respectively, in maximum acceleration in a touch-evoke response assay at 2 dpf compared to control zebrafish injected with a GFP targeting morpholino (Cont).

(D and E) Antibody labeling of Ryroxd1 double morphants at 48 hpf (D) and 96 hpf (E) for Actinin2 and phalloidin show disruption of muscle structure compared to uninjected controls.

(E) At 96 hpf, Ryroxd1 double morphants show severe disruption of the musculature with remnants of fragmented muscle fibers evident (arrows).

For (A) and (C), error bars represent SEM for three independent replicate experiments comprising 15 fish in each, $^{**}p < 0.01$.

with fragmentation of the muscle fibers (Figure 8E) and, in some cases, loss of fiber integrity and accumulation of actin at the myosepta (Figure 9A). Consistent with the improvement in muscle performance, the severity of structural muscle defects was significantly reduced by co-injection of Ryroxd1 double morphants with wtPYROXD1-eGFP mRNA (Figure 9A), demonstrating that the phenotype is due to reduction of Ryroxd1.

To further investigate the muscle phenotype observed in the morphant embryos, we examined the muscle structure using electron microscopy. In morphant embryos, but not uninjected controls, we observed disintegration of the myofibrils with mitochondrial infiltration of the resulting space, loss of Z-disk structures, and the formation of electron dense, nemaline-like, bodies reminiscent of those observed in the human muscle biopsies (Figure 9E).

Discussion

This publication describes the oxidoreductase function of *PYROXD1* and identifies recessive variants in *PYROXD1* as a cause of early-onset myopathy characterized histologically by a combination of multiple internalized nuclei, with large zones of sarcomeric disorganization—often devoid of mitochondria and organelles, accumulations of thin filaments, thickened Z-bands, and desmin-positive inclusions (Figure 2). All affected individuals presented in infancy or early childhood (1–8 years) with slowly progressive symmetrical weakness affecting both proximal and distal muscles, with normal to moderately elevated creatine kinase. Mild facial weakness, a high palate, nasal speech, and swallowing difficulties were typical features, mild restrictive lung disease was common, and evidence of cardiac involvement was present in the eldest individual, now aged 27. Thus, we emphasize the need for respiratory and cardiac surveillance in individuals with PYROXD1 myopathy. Nerve conduction studies in family A in the third decade showed a mild length-dependent axonal sensory neuropathy. These findings were present only in family A, so the significance is uncertain, but raises the possibility that different

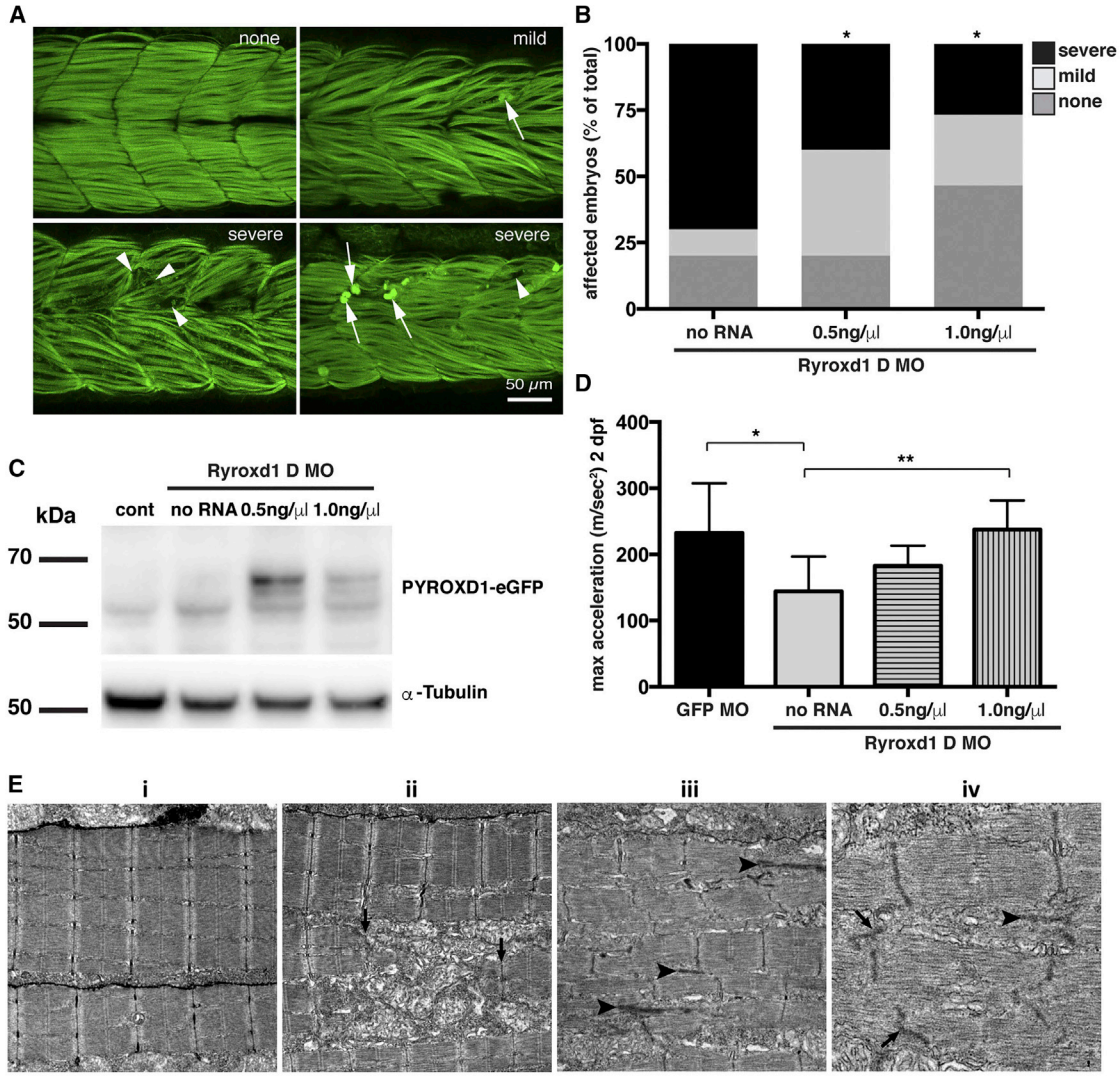

Figure 9. Human PYROXD1 Rescues Muscle Pathology and Swimming Defects in Ryroxd1 Morphants and EM of Zebrafish Muscle Pathology

(A) Representative images depicting the range of severity of muscle defects in Ryroxd1 double morphants. No obvious phenotype (none), embryos displaying occasional broken fibers and actin accumulation (mild, arrows), severe fragmentation of muscle fibers (severe, arrowheads), severe loss of fiber integrity and accumulation of actin at the myosepta (severe, arrows).

(B) Quantification of phenotypes (as in A) observed in Ryroxd1 double morphants (Ryroxd1 D MO) injected with either 0.5 ng/μL or 1.0 ng/μL wild-type (wt) wtPYROXD1-eGFP RNA compared to Ryroxd1 double morpholino injection alone (no RNA). 15–20 animals were scored per condition, *$p < 0.05$.

(C) Western blot for GFP and α-tubulin in GFP morpholino-injected control embryos (cont), Ryroxd1 double morpholino-injected zebrafish (no RNA), and Ryroxd1 double morpholino-injected zebrafish co-injected with either 0.5 ng/μL or 1.0 ng/μL wtPYROXD1-eGFP RNA, demonstrating translation of the injected mRNA.

(D) Ryroxd1 double morphants injected with human wtPYROXD1-eGFP mRNA show dose-dependent rescue in a touch-evoke response assay at 2 dpf. Ryroxd1 double morphants injected with 1.0 ng/μL human wtPYROXD1-eGFP show a 61% increase in maximum acceleration compared to Ryroxd1 double morphants (no RNA), achieving similar levels of maximum acceleration to wild-type embryos injected with a control GFP targeting morpholino (GFP MO).

(E) Electron micrograph of muscle (*i*) in a wild-type uninjected 96 hpf zebrafish embryo; examination of Ryroxd1 double morphant embryos (*ii–iv*) demonstrates myofibrillar fragmentation (*ii*, arrows) with mitochondrial infiltration, small nemaline-like bodies (*iii*, black arrowheads), and Z-disk fragmentation and loss (*iii–iv*; black arrowheads).

Scale bar represents 1 μm. Error bars represent SEM for three independent replicate experiments comprising 15 animals in each replicate experiment, *$p < 0.05$, **$p < 0.01$.

PYROXD1 variants may eventually predispose to the development of a neuropathy with increasing age.

All families identified in this study for which muscle, myoblasts, or fibroblasts were available exhibited either normal levels or reduced levels of PYROXD1; no individual showed absence of PYROXD1. Analysis of splice variants identified in *PYROXD1* in family A and family C revealed a subset of transcripts with in-frame deletion of amino acid sequences encoded by exon 3 (family A) or exon 4 (family C). However, we could not find evidence for

expression of truncated proteins, suggesting that the resulting protein products are unstable and degraded. The two substitutions p.Asn155Ser and p.Gln372His strongly impair the oxidoreductase activity of PYROXD1 in a yeast heterologous expression system. Importantly, no affected individuals described to date possess two predicted loss-of-function variants or exhibited complete loss of PYROXD1 in skin fibroblasts or skeletal muscle specimens. Thus, our findings suggest that myopathy results from partial loss of PYROXD1 function. Of note, targeted deletion of *PYROXD1* in murine models results in embryonic lethality (our own studies and confirmed by the International Mouse Phenotyping Consortium). This suggests that recessive loss-of-function variants in *PYROXD1* may result in a severe-lethal presentation in humans. Our current studies are defining the tissue-specific and developmental expression of PYROXD1, together with determination of the consequences of PYROXD1 deficiency, using a PYROXD1 conditional knock-out and LacZ reporter mouse-model.

PYROXD1 mRNA is ubiquitously expressed at low levels (GTex Portal). *PYROXD1* is highly evolutionarily conserved to unicellular eukaryotes, with functional FAD-dependent oxidoreductase and NADH-dependent nitrile reductase domains present in prokaryotic enzymes. Thus, PYROXD1 has an ancient biology not yet understood. In contrast to PYROXD1, the five other class I PNDRs are well characterized and play significant roles in regulation of cellular redox: glutathione reductase (*GSR*), thioredoxin reductases 1, 2, and 3 (*TXNRD1*, *TXNRD2*, and *TXNRD3*), and mitochondrial dihydrolipoyl dehydrogenase (*DLD*).[6] Recessive variants in *DLD* cause dihydrolipoamide dehydrogenase deficiency (DLDD [MIM: 246900]), a metabolic disorder characterized by lactic acidosis and neurological dysfunction. Dihydrolipoamide dehydrogenase is the E3 component of several vital mitochondrial enzyme complexes, including pyruvate dehydrogenase and ketoglutarate dehydrogenase, affecting oxidative metabolism via both the citric acid cycle and fatty acid biosynthesis.[6]

In addition to the reducing capabilities of their enzyme co-factors (FAD and NAD), PNDRs typically bear an intrinsic "redox active site" that catalyzes the final step to reduce their substrate, most commonly a conserved redox-reactive disulphide motif. Many PNDRs form enzymatic homodimers via a C-terminal conserved motif and are grouped into two classes (class 1 and class 2), according to characteristics related to nucleotide and flavin binding sites, the type of non-flavin redox active site, and the structural features of their dimer interface.[34] Although PYROXD1 is classified as a class 1 PNDR, it does not contain a conserved redox active disulphide within the oxidoreductase domain, nor a classical C-terminal dimerization motif, and thus appears a divergent member of the class I PNDR family.

Importantly, using a heterologous complementation assay in yeast, we showed that human PYROXD1 exhibits a reductase activity that can rescue the H_2O_2 sensitivity of yeast cells lacking the glutathione reductase *glr1*. As the two missense variants impair this activity, it supports that the myopathy observed in affected individuals arises, at least in part, from a defect in oxidoreductase activity. Future work will need to identify what are the substrate(s) of PYROXD1 to better understand the pathophysiology.

Immunolocalization studies in human skeletal muscle, skin fibroblasts, and zebrafish myofibers show that PYROXD1 localizes to both the nucleus and cytoplasmic/sarcomeric compartments. Knockdown of the zebrafish ortholog Ryroxd1 produced embryos with abnormal musculature and marked sarcomeric disorganization within individual myofibrils, including Z-disk loss and fragmentation and the presence of electron-dense bodies, reminiscent of findings observed in human muscle biopsies. In addition to the pathological features observed, Ryroxd1 morphants also performed poorly in a touch-evoked swim assay, consistent with impaired muscle function.

In summary, we describe PYROXD1 as a nuclear-cytoplasmic oxidoreductase conserved through evolution and important for human skeletal muscle biology. Recessive variants in *PYROXD1* cause an early-onset myopathy characterized by slowly progressive limb and facial weakness, nasal speech, and swallowing difficulties. PYROXD1 myopathy histopathology is distinctive in that it combines multiple pathological hallmarks characteristic of different myopathies: central core and minicore disease, centronuclear, myofibrillar, and nemaline myopathies. Although one or two of these histopathological features can often exist in combination, it is rare to observe core-like zones, multiple internal nuclei, extensive myofibrillar disorganization, myofibrillar accumulations, and small nemaline-like bodies all within a single biopsy specimen. Thus, our discovery of PYROXD1 myopathy introduces altered redox regulation as a primary disease mechanism in congenital myopathy and raises the provocative possibility that several pathological endpoints in the myopathies may be linked ultimately to altered cellular redox.

Supplemental Data

Supplemental Data include five case reports, one figure, and three tables and can be found with this article online at http://dx.doi.org/10.1016/j.ajhg.2016.09.005.

Acknowledgments

This study was supported by the following funding: The Australian National Health and Medical Research Council (NHMRC) 1080587 (S.T.C., N.F.C., D.G.M., K.N.N., R.B.R., K.J.N., N.G.L.), 1022707 and 1031893 (K.N.N., N.F.C., and N.G.L.), 1048816 (S.T.C.), and 1056285 (G.L.O.), Muscular Dystrophy New South Wales (G.L.O.), Royal Australasian College of Physicians (G.L.O.), Australian Research Council FT100100734 (K.J.N.), National Human Genome Research Institute of the NIH (D.G.M., Medical Sequencing Program grant U54 HG003067 to the Broad Institute principal investigator, Lander), Division of Intramural

Research of the National Institutes of Neurological Disorders and Stroke, France Génomique National infrastructure grant Investissements d'Avenir and Agence Nationale pour la Recherche (ANR-10-INBS-09 and ANR-11-BSV1-026), Fondation Maladies Rares "Myocapture" sequencing project, Association Française contre les Myopathies (AFM-15352 and AFM-16551), Muscular Dystrophy Association (MDA-186985), Myotubular Trust and IDEX-Université de Strasbourg PhD fellowship (M.S.-V.), and intramural funds of the NINDS/NIH (C.G.B. and S.D.).

We thank Sarah Sandaradura for recruitment and consent of family A, Meganne E. Leach for clinical review of family C, Goknur Haliloglu for clinical review of family D, Xavière Lornage and Christine Kretz for help with experiments for family B, Pierre Bouche and Gisèle Bonne for sequence analysis in family B, Roberto Silva Rojas for help with yeast experiments, and Maud Beuvin, Guy Brochier, and Dr. Edoardo Malfatti from the Morphological Unit of the Myology Institute (Paris).

Received: April 27, 2016
Accepted: September 7, 2016
Published: October 13, 2016

Web Resources

Clustal Omega, http://www.ebi.ac.uk/Tools/msa/clustalo/
dbSNP, http://www.ncbi.nlm.nih.gov/projects/SNP/
ExAC Browser, http://exac.broadinstitute.org/
GenBank, http://www.ncbi.nlm.nih.gov/genbank/
GeneTable of Neuromuscular Disorders, http://www.musclegenetable.fr/
GTEx Portal, http://www.gtexportal.org/home/gene/PYROXD1
Human Phenotype Ontology (HPO), http://www.human-phenotype-ontology.org/
International Mouse Phenotyping Consortium, http://www.mousephenotype.org/data/genes/MGI:2676395#section-associations
Knockout Mouse Project (KOMP) Repository, https://www.komp.org/
neXtprot, https://www.nextprot.org/term/FA-00613/
NHLBI Exome Sequencing Project (ESP) Exome Variant Server, http://evs.gs.washington.edu/EVS/
OMIM, http://www.omim.org/
RCSB Protein Data Bank, http://www.rcsb.org/pdb/home/home.do
RRID, https://scicrunch.org/resources
seqr, https://seqr.broadinstitute.org/
Sequence Manipulation Suite, http://www.bioinformatics.org/sms2/ident_sim.html
UniProt, http://www.uniprot.org/

References

1. Nance, J.R., Dowling, J.J., Gibbs, E.M., and Bönnemann, C.G. (2012). Congenital myopathies: an update. Curr. Neurol. Neurosci. Rep. *12*, 165–174.
2. Amburgey, K., McNamara, N., Bennett, L.R., McCormick, M.E., Acsadi, G., and Dowling, J.J. (2011). Prevalence of congenital myopathies in a representative pediatric united states population. Ann. Neurol. *70*, 662–665.
3. Chae, J.H., Vasta, V., Cho, A., Lim, B.C., Zhang, Q., Eun, S.H., and Hahn, S.H. (2015). Utility of next generation sequencing in genetic diagnosis of early onset neuromuscular disorders. J. Med. Genet. *52*, 208–216.
4. Ng, S.B., Buckingham, K.J., Lee, C., Bigham, A.W., Tabor, H.K., Dent, K.M., Huff, C.D., Shannon, P.T., Jabs, E.W., Nickerson, D.A., et al. (2010). Exome sequencing identifies the cause of a mendelian disorder. Nat. Genet. *42*, 30–35.
5. Ng, S.B., Nickerson, D.A., Bamshad, M.J., and Shendure, J. (2010). Massively parallel sequencing and rare disease. Hum. Mol. Genet. *19* (R2), R119–R124.
6. Argyrou, A., and Blanchard, J.S. (2004). Flavoprotein disulfide reductases: advances in chemistry and function. In Progress in Nucleic Acid Research and Molecular Biology (Academic Press), pp. 89–142.
7. Ghaoui, R., Cooper, S.T., Lek, M., Jones, K., Corbett, A., Reddel, S.W., Needham, M., Liang, C., Waddell, L.B., Nicholson, G., et al. (2015). Use of whole-exome sequencing for diagnosis of limb-girdle muscular dystrophy: outcomes and lessons learned. JAMA Neurol. *72*, 1424–1432.
8. Geoffroy, V., Pizot, C., Redin, C., Piton, A., Vasli, N., Stoetzel, C., Blavier, A., Laporte, J., and Muller, J. (2015). VaRank: a simple and powerful tool for ranking genetic variants. PeerJ *3*, e796.
9. Teer, J.K., Bonnycastle, L.L., Chines, P.S., Hansen, N.F., Aoyama, N., Swift, A.J., Abaan, H.O., Albert, T.J., Margulies, E.H., Green, E.D., et al.; NISC Comparative Sequencing Program (2010). Systematic comparison of three genomic enrichment methods for massively parallel DNA sequencing. Genome Res. *20*, 1420–1431.
10. Wang, K., Li, M., and Hakonarson, H. (2010). ANNOVAR: functional annotation of genetic variants from high-throughput sequencing data. Nucleic Acids Res. *38*, e164.
11. Thompson, J.D., Higgins, D.G., and Gibson, T.J. (1994). CLUSTAL W: improving the sensitivity of progressive multiple sequence alignment through sequence weighting, position-specific gap penalties and weight matrix choice. Nucleic Acids Res. *22*, 4673–4680.
12. Dereeper, A., Audic, S., Claverie, J.-M., and Blanc, G. (2010). BLAST-EXPLORER helps you building datasets for phylogenetic analysis. BMC Evol. Biol. *10*, 8.
13. Dereeper, A., Guignon, V., Blanc, G., Audic, S., Buffet, S., Chevenet, F., Dufayard, J.-F., Guindon, S., Lefort, V., Lescot, M., et al. (2008). Phylogeny.fr: robust phylogenetic analysis for the non-specialist. Nucleic Acids Res. *36*, W465-9.
14. Webb, B., and Sali, A. (2002). Comparative protein structure modeling using MODELLER. In Current Protocols in Bioinformatics (John Wiley & Sons, Inc.).
15. Pei, J., Kim, B.-H., and Grishin, N.V. (2008). PROMALS3D: a tool for multiple protein sequence and structure alignments. Nucleic Acids Res. *36*, 2295–2300.
16. Xu, D., and Zhang, Y. (2011). Improving the physical realism and structural accuracy of protein models by a two-step atomic-level energy minimization. Biophys. J. *101*, 2525–2534.
17. Wass, M.N., Kelley, L.A., and Sternberg, M.J.E. (2010). 3DLigandSite: predicting ligand-binding sites using similar structures. Nucleic Acids Res. *38*, W469-73.
18. Yuen, M., Sandaradura, S.A., Dowling, J.J., Kostyukova, A.S., Moroz, N., Quinlan, K.G., Lehtokari, V.-L., Ravenscroft, G., Todd, E.J., Ceyhan-Birsoy, O., et al. (2014). Leiomodin-3 dysfunction results in thin filament disorganization and nemaline myopathy. J. Clin. Invest. *124*, 4693–4708.
19. Sztal, T.E., Zhao, M., Williams, C., Oorschot, V., Parslow, A.C., Giousoh, A., Yuen, M., Hall, T.E., Costin, A., Ramm, G., et al.

(2015). Zebrafish models for nemaline myopathy reveal a spectrum of nemaline bodies contributing to reduced muscle function. Acta Neuropathol. *130*, 389–406.
20. Redpath, G.M.I., Sophocleous, R.A., Turnbull, L., Whitchurch, C.B., and Cooper, S.T. (2016). Ferlins show tissue-specific expression and segregate as plasma membrane/late endosomal or trans-Golgi/recycling ferlins. Traffic *17*, 245–266.
21. Gietz, D., St Jean, A., Woods, R.A., and Schiestl, R.H. (1992). Improved method for high efficiency transformation of intact yeast cells. Nucleic Acids Res. *20*, 1425.
22. Westerfield, M. (2007). The Zebrafish Book. A Guide for the Laboratory Use of Zebrafish (*Danio rerio*), Fifth Edition (Eugene: University of Oregon Press).
23. Higashijima, S., Okamoto, H., Ueno, N., Hotta, Y., and Eguchi, G. (1997). High-frequency generation of transgenic zebrafish which reliably express GFP in whole muscles or the whole body by using promoters of zebrafish origin. Dev. Biol. *192*, 289–299.
24. Sztal, T.E., Sonntag, C., Hall, T.E., and Currie, P.D. (2012). Epistatic dissection of laminin-receptor interactions in dystrophic zebrafish muscle. Hum. Mol. Genet. *21*, 4718–4731.
25. Ruparelia, A.A., Oorschot, V., Ramm, G., and Bryson-Richardson, R.J. (2016). FLNC myofibrillar myopathy results from impaired autophagy and protein insufficiency. Hum. Mol. Genet., ddw080.
26. Ruparelia, A.A., Zhao, M., Currie, P.D., and Bryson-Richardson, R.J. (2012). Characterization and investigation of zebrafish models of filamin-related myofibrillar myopathy. Hum. Mol. Genet. *21*, 4073–4083.
27. Lek, M., Karczewski, K., Minikel, E., Samocha, K., Banks, E., Fennell, T., O'Donnell-Luria, A., Ware, J., Hill, A., Cummings, B., et al. (2015). Analysis of protein-coding genetic variation in 60,706 humans. bioRxiv http://dx.doi.org/10.1038/nature19057.
28. Adzhubei, I.A., Schmidt, S., Peshkin, L., Ramensky, V.E., Gerasimova, A., Bork, P., Kondrashov, A.S., and Sunyaev, S.R. (2010). A method and server for predicting damaging missense mutations. Nat. Methods *7*, 248–249.
29. Kumar, P., Henikoff, S., and Ng, P.C. (2009). Predicting the effects of coding non-synonymous variants on protein function using the SIFT algorithm. Nat. Protoc. *4*, 1073–1081.
30. Schwarz, J.M., Rödelsperger, C., Schuelke, M., and Seelow, D. (2010). MutationTaster evaluates disease-causing potential of sequence alterations. Nat. Methods *7*, 575–576.
31. Amoasii, L., Bertazzi, D.L., Tronchère, H., Hnia, K., Chicanne, G., Rinaldi, B., Cowling, B.S., Ferry, A., Klaholz, B., Payrastre, B., et al. (2012). Phosphatase-dead myotubularin ameliorates X-linked centronuclear myopathy phenotypes in mice. PLoS Genet. *8*, e1002965.
32. Kachroo, A.H., Laurent, J.M., Yellman, C.M., Meyer, A.G., Wilke, C.O., and Marcotte, E.M. (2015). Evolution. Systematic humanization of yeast genes reveals conserved functions and genetic modularity. Science *348*, 921–925.
33. Trotter, E.W., and Grant, C.M. (2005). Overlapping roles of the cytoplasmic and mitochondrial redox regulatory systems in the yeast *Saccharomyces cerevisiae*. Eukaryot. Cell *4*, 392–400.
34. Kuriyan, J., Krishna, T.S.R., Wong, L., Guenther, B., Pahler, A., Williams, C.H., Jr., and Model, P. (1991). Convergent evolution of similar function in two structurally divergent enzymes. Nature *352*, 172–174.
35. Liu, W., Xie, Y., Ma, J., Luo, X., Nie, P., Zuo, Z., Lahrmann, U., Zhao, Q., Zheng, Y., Zhao, Y., et al. (2015). IBS: an illustrator for the presentation and visualization of biological sequences. Bioinformatics *31*, 3359–3361.